CHALMERS
UNIVERSITY OF TECHNOLOGY

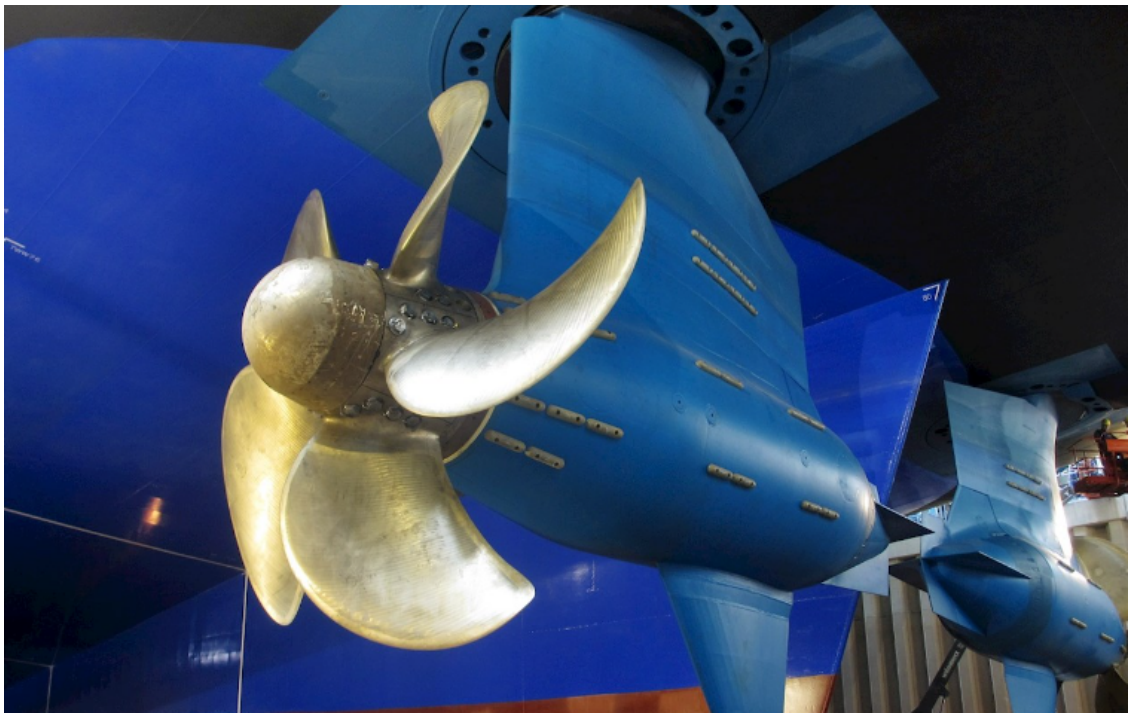

Design and analysis of a low speed and high power permanent magnet synchronous motor for a ship's pod

Performance comparison of the electromagnetic, thermal, mechanical and environmental aspects of Neodymium and Ferrite machine

Sustainable Electric Power Engineering and Electromobility

Jinzhe Yang
Muhammad Irsyadul Umami

DEPARTMENT OF Electrical Engineering
CHALMERS UNIVERSITY OF TECHNOLOGY
Gothenburg, Sweden 2024
www.chalmers.se

Master's thesis 2024

Design and analysis of a low speed and high power permanent magnet synchronous motor for a ship's pod

Performance comparison of the electromagnetic, thermal, mechanical and environmental aspects of Neodymium and Ferrite machine

Jinzhe Yang
Muhammad Irsyadul Umami

CHALMERS
UNIVERSITY OF TECHNOLOGY

Department of Electrical Engineering
Division of Electric Power Engineering
Chalmers University of Technology
Gothenburg, Sweden 2024

Design and analysis of a low speed and high power permanent magnet synchronous motor for a ship's pod
Performance comparison of the electromagnetic, thermal, mechanical and environmental aspects of Neodymium and Ferrite machine
Jinzhe Yang
Muhammad Irsyadul Umami

Supervisor: Torbjörn Thiringer, Department of Electrical Engineering, Chalmers
Examiner: Torbjörn Thiringer, Department of Electrical Engineering, Chalmers

Master's Thesis 2024
Department of Electrical Engineering
Division of Electric Power Engineering
Chalmers University of Technology
SE-412 96 Gothenburg
Telephone +46 31 772 1000

Cover: Demonstration of POD propulsion system in the cabin

Typeset in LaTeX
Printed by Chalmers Reproservice
Gothenburg, Sweden 2024

Design and analysis of a low speed and high power permanent magnet synchronous motor for a ship's pod
Performance comparison of the electromagnetic, thermal, mechanical and environmental aspect of Neodymium and Ferrite machine
Jinzhe Yang
Muhammad Irsyadul Umami
Department of Electrical Engineering
Chalmers University of Technology

Abstract

The route between Gothenburg Port and Frederikshavn Port requires a ship propulsion system capable of delivering 200 kNm torque at 75 RPM. A Permanent Magnet Synchronous Motor (PMSM) is designed for this purpose, with Motor-CAD employed for comprehensive simulations, including geometric design and parameter optimization. The motor, rated at 1568 kW with a maximum current of 800 A, incorporates advanced design considerations to enhance performance.

Magnet material selection plays a crucial role in determining the motor's efficiency and losses. A comparison between the ferrite and the neodymium magnets reveals that the neodymium achieves a higher efficiency of 95.9% compared to 94.1% for the ferrite. Additionally, the neodymium results in significantly lower total losses of 64.19 kW, compared to 95.34 kW for the ferrite, demonstrating superior electromagnetic performance.

To address thermal challenges, seawater heat dissipation is implemented as an effective cooling strategy, ensuring optimal system performance. Mechanical stress simulations further guarantee the safety and reliability of the vessel. A life cycle assessment (LCA) evaluates the environmental sustainability of the propulsion system, covering every phase from material selection to decommissioning.

This work integrates thermal management, structural analysis, and sustainability to deliver an efficient and environmentally friendly marine propulsion system, offering valuable insights for the development of next-generation ship technologies.

Keywords: PMSM, Motorcad, marine propulsion, Ferrite, Neodymium, LCA.

Acknowledgements

The successful completion of this thesis is inseparable from the guidance and help of Chalmers University and Professor Torbjörn. Here, we would like to express our sincerest gratitude to all those who have supported and helped me. Chalmers University has provided us with a good research environment, which has enabled the research work of this thesis to proceed smoothly. Professor Torbjörn provided careful guidance and unremitting encouragement in the selection of the thesis topic, the establishment of research ideas, and the writing process of the thesis. His academic rigor and innovative spirit have benefited us a lot. Thanks to all those who have helped us, and We would like to express our sincerest respect to them through this thesis report.

Jinzhe Yang
Muhammad Irsyadul Umam
Gothenburg, 2024

List of Acronyms

AC	Alternating Current
DC	Direct Current
EPS	Environmental Priority Strategies
Fe	Ferrite
GWP	Global Warming Potential
Hz	Hertz
IPMSM	Interior Permanent Magnet Synchronous Machine
MTPA	Maximum Torque per Ampere
Nd	Neodymium
NdFeB	Neodymium Iron Boron
PMSM	Permanent Magnet Synchronous Machine
PWM	Pulse Width Modulation
RPM	Revolutions per Minute
SMPMSM	Surface-Mounted Permanent Magnet Synchronous Machine

Nomenclature

α	Exponential Factor for Hysterisi Loss
η	Efficiency of the Propeller (%)
ν	Kinematic Viscosity of Water (m^2/s)
Ω_r	Angular Velocity of the Rotor (rad/s)
ψ_d	Stator Flux Linkage in d-axis (Wb)
ψ_{pm}	Stator Flux Linkage of Permanent Magnet (Wb)
ψ_q	Stator Flux Linkage in q-axis (Wb)
ρ	Resistivity of Conductor (Ohm.m)
ρ_{water}	Density of Water (kg/m^3)
σ	Rotor Lamination Stress (MPa)
A_{cond}	Area of Conductor (mm^2)
A_{slot}	Area of Slot (mm^2)
B	Magnetic Flux Density (Tesla)
$cos\phi$	Power Factor
C_f	Frictional Resistance Coefficient
F_{ship}	Ship Force (kN)
i_d	Stator Current in d-axis (Amps)
i_{max}	Current Limit
i_q	Stator Current in q-axis (Amps)
$I_{max,rms}$	Maximum Current RMS (Amps)
J	Current Density ($Amps/mm^2$)
k_{eddy}	Eddy Loss Coefficient
k_{fill}	Fill factor
k_h	Hysterisis Loss Coefficient
l_{active}	Length of Conductor in Machine's Active Part (mm)

l_{EW}	Length of End Winding (mm)
l_{turn}	Total length of conductor (m)
L_{cond}	Height of Conductor (mm)
L_d	Inductances in d-axis (mH)
L_q	Inductances in q-axis (mH)
L_{WL}	Length of the Hull (m)
m	Number of phases
n_p	Number of Pole Pairs
n_s	Synchronous Speed (RPM)
$N_{conductor}$	Number of Conductors
N_p	Number of Poles
N_{strand}	Number of Conductor Strands
P	Power of the Ship (MW)
P_{cu}	Stator Copper Loss (kW)
P_e	Electromagnetic Power (MW)
P_{eddy}	Eddy Loss (kW)
P_{fe}	Iron Losses (kW)
P_h	Hysteresis Loss (kW)
P_{shaft}	Shaft Power of the ship (MW)
q	Number of Slots per pole per phase
Q_s	Number of Slots
r	Insulation thickness (mm)
R	Phase Resistance (Ohms)
R_e	Reynolds Number
R_s	Stator Winding Resistance (Ohm)
S	Waterline Area of the Hull (m^2)
SCF	Stress Concentration Factor
SF	Safety Factor
T_e	Electromagnetic Torque (Nm)
u_d	Stator Voltage in d-axis (Volts)
u_q	Stator Voltage in q-axis (Volts)
v_{ship}	Velocity of the Ship
$V_{line,peak}$	Line Phase Voltage (Volts)
W_{cond}	Width of the Conductor (mm)

Contents

List of Acronyms viii

Nomenclature xi

1 Introduction 1
- 1.1 Background . . . 1
- 1.2 Previous work . . . 1
- 1.3 Purpose . . . 2

2 Theory 3
- 2.1 Ship propulsion . . . 3
- 2.2 Permanent Magnet Synchronous Motor . . . 4
  - 2.2.1 Mathematical model . . . 5
  - 2.2.2 Current limit . . . 6
  - 2.2.3 Voltage limit . . . 6
  - 2.2.4 Voltage, Current and Power calculation . . . 7
- 2.3 Winding and other parameters of the machine . . . 8
- 2.4 Losses and Efficiency . . . 9
  - 2.4.1 Copper Losses . . . 9
  - 2.4.2 Iron Losses . . . 10
  - 2.4.3 Mechanical Losses . . . 10
  - 2.4.4 Efficiency of the motor . . . 11
- 2.5 Cooling system . . . 11
- 2.6 Environment impact of the Neodymium and the Ferrite . . . 11

3 Methods 13
- 3.1 Operation and Characteristic of the Ship . . . 13
  - 3.1.1 Characteristic of the ship for the propulsion system . . . 14
- 3.2 Configuration and components of pod propulsion systems . . . 16
- 3.3 Electric Constraints . . . 17
- 3.4 Parameters of the machine . . . 17
- 3.5 Geometry of the motor . . . 18
- 3.6 The material selection . . . 19
- 3.7 Thermal and cooling setting . . . 21

4 Analysis 25
- 4.1 The machine electromagnetic simulation results . . . 25

4.2 The winding of the machine 26
4.3 Flux density of the machines 29
4.4 Torque-speed plot and MTPA trajectory 31
4.5 Temperature of the Machines 32
4.6 Losses and Efficiency of the Machines 35
4.6.1 Losses of the machines 35
4.6.2 Efficiency of the machines 37
4.7 Comparison of drive cycle performances of the machines 38
4.8 Mechanical Simulation of the Machines 40
4.9 Environmental impact analysis 42
4.9.1 Environmental Priority Strategies (EPS) 43
4.10 Global warming potential analysis of the machines 44
4.11 Ethical impact 46

5 Conclusions **47**
5.1 Future Work 48

Bibliography **49**

A Material specification **I**

1
Introduction

1.1 Background

The permanent magnet synchronous machine (PMSM) is an advanced and highly efficient machine for pod propulsion systems, where the need for high torque at low speeds is crucial for direct-drive functionality. Some components include the stator, which contains windings that generate the rotating magnetic field, and the rotor, which incorporates permanent magnets that allow synchronous operation. These magnets can be made from ferrite or Neodymium materials, which influence the motor's overall performance, especially regarding power density and thermal behavior.

The Ferrite magnet performs at a lower power density. In contrast, the Neodymium magnets provide significantly higher magnetic flux density, allowing for a more compact and powerful motor design, which is typically chosen for high-performance applications. In pod propulsion systems, the selection between the ferrite and the Neodymium magnets is determined by the specific operational priorities, such as efficiency, power output, temperature distribution, and mechanical stress in the motor parts.

To manage the high power and torque demands, efficient cooling systems, such as water or air-based solutions, are vital, particularly when using the Neodymium magnets. These magnets are sensitive to overheating, necessitating careful thermal regulation. This design enables the PMSM to operate with high efficiency and reduced energy losses, making it an ideal choice for marine propulsion systems where reliability, extended operation, and energy efficiency are essential.

1.2 Previous work

Research on applying permanent magnet synchronous machines in pod propulsion systems has shown a better performance than induction machines. Replacing an induction machine with a PMSM significantly reduced energy losses while improving marine propulsion's power density and efficiency. PMSMs, with their ability to generate high torque at low speeds, were ideal for direct-drive configurations, allowing for the elimination of gearboxes and associated mechanical losses[1].

Various studies have also explored further advancements in the thermal and electro-

magnetic optimization of the PMSM. The first study showed the challenge of heat generation in high-power PMSM, particularly the use of the Neodymium Iron Boron (NdFeB) magnets. The research investigated the optimization of rotor designs to reduce eddy current losses and improve the motor's thermal performance[2]. Another study proposed advanced cooling techniques, including liquid and air-cooled solutions, which were found to effectively mitigate thermal challenges in a PMSM used in harsh marine environments[3].

A comparative analysis between the Ferrite and Neodymium machine has been widely documented. The use of the ferrite magnets highlights their resilience to high temperatures, although their lower magnetic flux density limits the motor's torque and power density[4]. Conversely, the advantages of the Neodymium machine offers high torque output and compact designs suitable for high-performance for the ship. However, these motors required more sophisticated thermal management strategies[5].

1.3 Purpose

This thesis aims to produce designs of electrical permanent magnet synchronous machines, which will be used for propulsion systems in a pod. The output power of the machine design is 1.5 MW at a speed of 75 RPM. Moreover, the electromagnetic, thermal, and mechanical behavior will be studied. Apart from that, an analysis of the drive cycle characteristics will also be carried out in the report. Finally, there are two machine models of PMSM, the Neodymium and the Ferrite, to give comparison results and find a better machine design.

2
Theory

This part will discuss the theory behind the ship force, permanent magnet synchronous machine, the formula used to analyze the machine, types of losses reducing the efficiency of the ship propulsion system, machine and the cooling system, and environment impact of the Neodymium and the Ferrite material.

2.1 Ship propulsion

Ship propulsion is the process of driving a ship forward by converting a certain form of energy (electrical or chemical energy) into mechanical energy. The main goal of the propulsion system is to overcome the water resistance of the ship to make it move on the water. This is done by the propellers because the thrust generated by the propellers in the water can be used to offset the resistance in the water.

For the ship to maintain a constant speed, the thrust must be equal to the total resistance encountered by the ship as it moves forward. The total resistance includes the friction resistance between the hull and the water and the wave resistance caused by the waves generated by the hull breaking through the water surface. However, considering that the ship in this report is moving at low speed and in relatively calm waters, the wave resistance will not be considered. Regarding friction resistance, the relation between frictional resistance and speed can be determined as[6],

$$F_{ship} = \frac{1}{2}\rho_{water} S C_f v_{ship}^2 \tag{2.1}$$

where ρ_{water} is the density of water (kg/m^3), S is the waterline area of the hull (m^2), v_{ship} is the speed of the ship (m/s), and C_f is the frictional resistance coefficient, (dimensionless), depends on the hull shape and flow conditions. C_f can be found as[6],

$$C_f = \frac{0.075}{(\log_{10}(R_e) - 2)^2} \tag{2.2}$$

where R_e represents the Reynolds number, defined as[6],

$$R_e = \frac{v_{ship} L_{WL}}{\nu} \tag{2.3}$$

where v_{ship} refers to the ship's velocity in meters per second (m/s), L_{WL} is the length of the hull at the waterline in meters (m), ν means kinematic viscosity of

water, typically measured in (m^2/s). Generally, at a water temperature of 20°C, the kinematic viscosity is 1.04 $\times 10^{-6}$ m^2/s.

The power required for a ship to move forward is determined by the ship's horizontal speed (m/s) and the Horizontal force (kN). This power is used to drive the ship forward during the operation. By determining the efficiency of the propeller, the ship's power can be expressed as,

$$P = F_{ship}\ v_{ship} \tag{2.4}$$

$$P_{shaft} = P\ \eta_{propeller} \tag{2.5}$$

2.2 Permanent Magnet Synchronous Motor

Permanent magnet synchronous machines (PMSMs) are a type of electric motors utilizing the permanent magnets embedded in or attached to the rotor to create a constant magnetic field, enabling efficient and precise control of torque and speed. These machines have become the primary choice in various industrial applications, such as electric vehicles, robotics, and renewable energy systems, due to high efficiency, reliability, and excellent performance. The PMSM operates on the principle of synchronous rotation, where the rotor's magnetic field locks in synchronization with the rotating magnetic field produced by the stator windings. PMSMs are typically composed of three main components: the stator, the rotor, and the permanent magnets.

Stator: This is the stationary part of the motor, which consists of laminated steel cores with embedded copper windings. These windings are usually three-phase and are responsible for producing a rotating magnetic field when an AC supply is applied.

Rotor: This is the rotating component that houses the permanent magnets. This part can be designed in several configurations, such as surface-mounted magnets (SMPMSM) or interior permanent magnets (IPMSM). The choice of rotor configuration affects the motor's performance characteristics, including torque capability and field-weakening potential.

Permanent Magnets: This is typically made of rare-earth materials, such as the Neodymium (Nd) or Ferrite (Fe), which provide a high magnetic field density and contribute to the motor's compact design and high efficiency.

PMSMs offer several advantages that make them suitable for a wide range of applications:

High Efficiency: Using permanent magnets eliminates the need for rotor winding excitation, reducing copper losses and enhancing efficiency.

Compact Size: The high energy density of rare-earth magnets allows for a compact motor design, making PMSMs ideal for applications with space constraints.

Excellent Dynamic Performance: PMSMs provide high torque density and fast response, enabling precise control of speed and position.

Low Maintenance: The absence of brushes and slip rings reduces maintenance requirements and enhances the reliability of the motor.

PMSMs are widely used in various applications due to their superior performance characteristics. Some common applications include:

Electric Vehicles: PMSMs are used in electric and hybrid vehicles for their high efficiency and compact size, contributing to extended driving range and reduced energy consumption.

Industrial Automation: PMSMs are employed in robotics, CNC machines, and industrial automation systems for their precise control and dynamic response.

Renewable Energy: PMSMs are used in wind turbines and solar tracking systems due to their high efficiency and reliability in variable-speed applications.

Home Appliances: PMSMs are found in household appliances such as washing machines and air conditioners for their quiet operation and energy efficiency.

2.2.1 Mathematical model

In general, analyzing a permanent magnet synchronous motor can be represented in a dq-coordinated system in which the dq-system is a rotating reference system. The voltage equations in the stator frame can be expressed as[7],

$$u_d = R_s i_d + \frac{d\psi_d}{dt} - \omega_r \psi_q \tag{2.6}$$

$$u_q = R_s i_q + \frac{d\psi_q}{dt} + \omega \psi_d \tag{2.7}$$

$$u_0 = R_s i_0 + \frac{d\psi_0}{dt} \tag{2.8}$$

where u_d, u_q, and u_0 are the stator voltages, R_s is the stator winding resistance, i_d, i_q, and i_0 are the stator currents, ψ_d, ψ_q, and ψ_0 are the stator flux linkages, and ω_r is the electrical angular velocity of the rotor.

The zero-sequence components can be neglected due to the absence of a balanced three-phase system. Thus, this is simplified by modeling in two equations, (2.6) and (2.7).

The stator flux linkages in the dq-coordinate can be defined as[7],

$$\psi_d = L_d i_d + \psi_{pm} \tag{2.9}$$

$$\psi_q = L_q i_q \tag{2.10}$$

where L_d and L_q are the inductances of stator windings, and ψ_{pm} and the flux linkage due to the permanent magnet.

The electromagnetic torque produced by the permanent magnet synchronous motor is defined by[7],

$$T_e = \frac{3n_p}{2}(\psi_d i_q - \psi_q i_d) \tag{2.11}$$

Finally, by substituting the (2.9)and (2.10), the electromagnetic torque can be expressed by[7],

$$T_e = \frac{P_e}{\Omega_r} = \frac{3n_p}{2}[(L_d i_d + \psi_{pm})i_q - L_q i_q i_d] \tag{2.12}$$

or,

$$T_e = \frac{P_e}{\Omega_r} = \frac{3n_p}{2}(\psi_{pm} i_q + (L_d - L_q)i_d i_q) \tag{2.13}$$

where n_p is the number of pole pairs. The term $(L_d - L_q)i_d i_q$ represents the reluctance torque, which arises due to the difference in inductance along the dq-axis.

2.2.2 Current limit

In the dq-coordinate system, the stator current can be defined as[7],

$$i_s = \sqrt{i_d^2 + i_q^2} \tag{2.14}$$

where i_d and i_q are the d-axis and q-axis of current components, respectively. The current limit is a constant value i_{max} that defines a circular boundary in the i_d and i_q plane[7],

$$i_{max} \geq \sqrt{i_d^2 + i_q^2} \tag{2.15}$$

Within this boundary, the current can vary in direction to achieve different operating points, but cannot exceed the maximum magnitude i_{max}.

2.2.3 Voltage limit

By using (2.6), (2.7), (2.9), and (2.10), the stator voltage can be defined as [6],

$$u_s^2 = u_d^2 + u_q^2 = (R_s i_d - \omega_r L_q i_q)^2 + (R_s i_q + \omega_r L_d i_d + \omega_r \psi_{pm})^2 \tag{2.16}$$

Then, the voltage drop of the stator winding can be neglected. It can be defined as [6],

$$\frac{u_s^2}{\omega_r^2} = (L_d i_d + \psi_{pm})^2 + (L_q i_q)^2 \tag{2.17}$$

$$\frac{(i_d + \frac{\psi_{pm}}{L_d})^2}{\frac{u_s^2}{\omega_r^2 L_d^2}} + \frac{i_q^2}{\frac{u_s^2}{\omega_r^2 L_q^2}} = 1 \tag{2.18}$$

For a maximum voltage $u_{s,max}$ the voltage limit is represented as an ellipse expression as[7],

$$\frac{(i_d + \frac{\psi_{pm}}{L_d})^2}{L_q^2} + \frac{i_q^2}{L_d^2} \leq (\frac{u_{s,max}}{\omega_r L_d L_q})^2 \tag{2.19}$$

(2.19) defines the maximum stator voltage $u_{s,\max}$ as $u_{dc}/\sqrt{3}$. On the d-q plane, the center of the voltage-limiting ellipse is located at $\left(-\frac{\psi_{PM}}{L_d}, 0\right)$, as shown in Fig. 2.1. This voltage limit, along with the current limit, creates a boundary for safe operation, which should not be exceeded to prevent machine damage. The speed at which the motor's current limit meets the maximum voltage limit is known as the base speed.

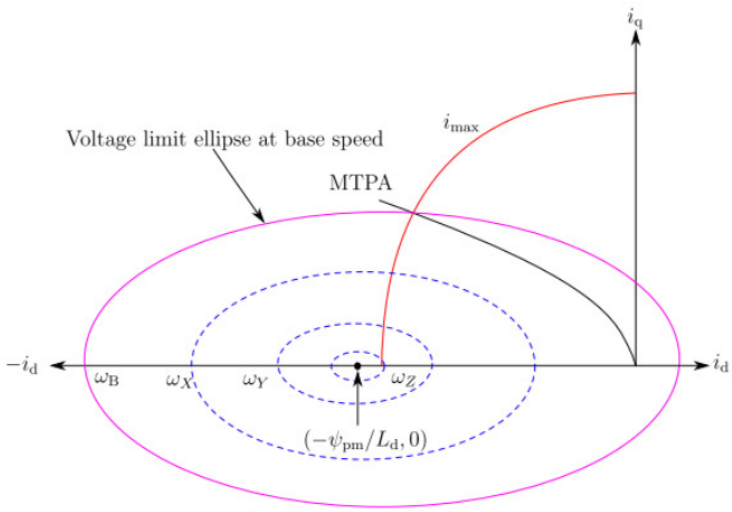

Figure 2.1: Current limit, voltage limit, and MTPA line[7]

2.2.4 Voltage, Current and Power calculation

First, in order to obtain the rms value of the motor line voltage, the DC bus voltage will be converted into the peak value of the phase voltage through modulation technology (sinusoidal pulse width modulation, Sinusoidal PWM). The specific formula can be expressed as,

$$V_{\text{phase, peak}} = \frac{V_{\text{dc}}}{\sqrt{3}} \tag{2.20}$$

Then, the conversion relationship between line voltage and phase voltage can be expressed as,

$$V_{\text{line, peak}} = \sqrt{3} \cdot V_{\text{phase, peak}} \tag{2.21}$$

Finally, since the result is the peak value of the line voltage, it is necessary to convert it again to get the rms value of the line voltage, which can be calculated by,

$$V_{\text{line, RMS}} = \frac{V_{\text{line, peak}}}{\sqrt{2}} \tag{2.22}$$

The general formula for calculating the output power of a three-phase motor can be determined as,

$$P_{\text{out}} = \sqrt{3} V_{\text{line}} I \cos\phi \tag{2.23}$$

where P_{out} is the output power (in watts or kilowatts), V_{line} is the line-to-line RMS voltage (in Volts), $\cos\phi$ is the power factor, which represents the phase angle difference between voltage and current.

2.3 Winding and other parameters of the machine

The relationship between synchronous speed and the number of poles in an electric motor is fundamental to motor design and operation. In general, the synchronous speed (n_s) of the motor depends on the frequency (f) and the number of poles (Np). This relation can be calculated using[7],

$$n_s = \frac{120f}{N_p} \tag{2.24}$$

When calculating the winding arrangement and distribution, the number of slots per pole per phase is also a key parameter, which can be expressed as[7],

$$Q_s = N_p m q \tag{2.25}$$

Then The motor slot area directly affects the electromagnetic and thermal performance of the motor. The effective slot area, which is the portion of the slot that can accommodate the winding conductor, can be calculated by using,

$$A_{slot} = \text{slot width(slot depth - tooth tip depth)} \tag{2.26}$$

Then, the area of a rectangular conductor can be calculated by using[8],

$$A_{cond} = (L_{cond} + 2r)(W_{cond} + 2r) - 4r^2 + \pi r^2 \tag{2.27}$$

where L_{cond} is the height of the conductor, W_{cond} is the width the conductor, r is the thickness of the insulator.

Next, the number of conductors per slot can be calculated by,

$$N_{cond} = \frac{A_{slot}}{A_{cond}} k_{fill} \tag{2.28}$$

Besides, winding length is an important part that can affect the phase of the resistance. The winding length consists of the windings in the active part and the end winding of the machines.

The length of the conductor (l_{turn}) used per pahse can be defined as[9],

$$l_{turn} = 2(l_{active} + l_{EW}) N_{cond} \tag{2.29}$$

As for the End winding turn length, it can be calculated by[9],

$$l_{EW} = 1.2\frac{\pi \text{ Stator inner diameter}}{N_p} \tag{2.30}$$

where l_{active} is the length of the conductor in the active motor part and l_{EW} is the length of the end winding part.

In the PMSM, current density is a crucial parameter because it can directly impact the copper loss. This type of loss is proportional to the square of the current density, defining it as a key factor to determine the machine's efficiency. The copper loss also depends on the conductor material's resistivity and the conductor's cross-sectional area. Then, the current density can be defined as[10],

$$J = \frac{I_{max,rms}}{A_{cond}\ N_{strand}} \tag{2.31}$$

2.4 Losses and Efficiency

Different sources of loss can be classified into several categories: Copper loss, iron loss, and mechanical loss. These losses generate heat which is an important factor to consider when designing electrical machines. In addition to thermal issues, power losses can result in financial costs due to energy waste and environmental issues.

2.4.1 Copper Losses

Losses resulting from current flowing within a conductor are referred to as copper losses. It is reliant on both the current density and resistance. This loss is sometimes also defined as the Ohmic loss or Winding loss. The copper losses include DC and AC losses.DC losses mean losses due to fundamental frequency, and AC losses are losses due to high frequency.

Then, the losses in a winding with m phases and current can be determined as[10],

$$P_{Cu} = mI^2R \tag{2.32}$$

where R is the phase resistance of the winding can be determined as[10],

$$R = \frac{\rho\ l_{turn}}{A_{cond}} \tag{2.33}$$

where ρ is defined as the conductor resistivity of the material used, l is the length of the conductor applied in the motor, and A is the cross-sectional area of the conductor.

Temperature can influence the phase resistance, specifically in the conductor resistivity, then it can be calculated as[10],

$$\rho(T) = \rho_0\left[1 + \alpha(T - T_0)\right] \tag{2.34}$$

where $\rho(T)$ is the resistivity at temperature T, ρ_0 is the resistivity at reference temperature T_0, and α is the temperature coefficient of resistivity.

2.4.2 Iron Losses

Iron loss mainly consists of two parts: hysteresis loss and eddy current loss. Hysteresis loss is due to the lag between the change of magnetizing force and the change of magnetizing intensity in the motor core material, which causes energy to be dissipated in the form of heat. By using the Steinmetz equation, the losses can be defined as[10],

$$P_h = k_h f B^\alpha \tag{2.35}$$

where k_h is the hysteresis loss coefficient, f is the frequency of the magnetic field in Hz, B is the magnetic flux density in Tesla, α is an exponential factor for hysteresis loss.

Eddy current loss is the resistance heat loss caused by the eddy current induced by the alternating magnetic field inside the conductive material[10],

$$P_{eddy} = k_{eddy} f^2 B^2 \tag{2.36}$$

where k_{eddy} is the eddy current loss coefficient, f is the frequency in Hz, and B is the magnetic flux density in Tesla. Then, K_h, K_{eddy}, and α are the Steinmetz coefficient.

Finally, total iron loss is the combination of hysteresis loss and eddy current loss[10],

$$P_{fe} = P_{hysteresis} + P_{eddy} \tag{2.37}$$

2.4.3 Mechanical Losses

Bearing friction and windage are two components that determined mechanical losses. The bearing friction is the losses that determined by speed of the shaft, type of the bearing used, lubricant and the load on the bearing that can be defined as[10],

$$P_{bearing} = 0.5\Omega\mu F D_{bearing} \tag{2.38}$$

where Ω is the mechanical speed of the machine, μ the coefficient of bearing friction, F the load of the bearing and $D_{bearing}$ the inner diameter of the bearing used in the machine.

On the other hand, the increasing speed of the machine can significantly affect the windage losses because of the friction between air around the rotational part of the machine and the surface of its rotational part. Then, it can be defined as[10],

$$P_{windage} = k_\rho D_r (l_r + 0.6\tau_p) v_r^2 \tag{2.39}$$

where k_ρ is the experimental factor of Schuisky, which is 8 for large machines, D_r is the rotor diameter, l_r is the rotor length, τ_p is the pole pitch and v_r^2 is the speed

of the rotor. Then, mechanical losses can be defined as the sum of the friction and windage loss[10],

$$P_{mech} = P_{bearing} + P_{windage} \tag{2.40}$$

2.4.4 Efficiency of the motor

The efficiency of the motor can be explained as the ratio between the output power and the input power[7],

$$\eta = \frac{OutputPower}{InputPower} = \frac{P_{in} - P_{cu} - P_{fe} - P_{mech}}{P_{in}} \tag{2.41}$$

where P_{out} is the mechanical power that can be read in the shaft of the motor, while the input power is the the electric power that can be read in the terminals.

2.5 Cooling system

The cooling system of this machine adopts submerged cooling[11]. This is because liquid has a higher heat capacity and thermal conductivity than air, which can remove heat more effectively, and submerged cooling ensures that all parts of the machine are cooled evenly. For the working principle of submerged cooling, the machine is generally immersed in a coolant, usually water or a special coolant. Here we use seawater, which absorbs the heat generated by the machine and carries it away, thus maintaining an acceptable operating temperature. In terms of ship design, the improved cooling efficiency of submersible cooling makes the machine design more compact, which is extremely helpful for space-constrained ship applications, so we adopted submersible cooling for this design.

2.6 Environment impact of the Neodymium and the Ferrite

When comparing the environmental impact of the ferrite and the Neodymium magnets, the Neodymium magnets (NdFeB) generally have a greater environmental impact due to the rare earth metals involved in their production. The mining of Neodymium requires large amounts of mining, especially in countries such as China, which leads to higher greenhouse gas emissions, large amounts of waste, and water pollution. It also stimulates increased greenhouse gas emissions, and increased water and land pollution caused by rare earth mining, and the complex manufacturing process requires more energy and produces toxic byproducts (such as hydrofluoric acid) [12].

In contrast, the Ferrite magnets (usually made from iron oxide) have a lower environmental impact due to the iron and ceramic-based components, more abundant raw materials, and simpler manufacturing processes[13]. Less energy is required during production and extraction. The waste is less toxic compared to the Neodymium. In

addition, ferrite magnets generally have lower energy and material inputs, resulting in fewer emissions.

Both magnets have their advantages in different application areas, but from an environmental sustainability perspective, the ferrite is a more environmentally friendly choice because it has fewer concerns about resource extraction and lower energy requirements during manufacturing. However, the neodymium magnets have superior magnetic strength and are hard to replace in applications that require high power density.

3
Methods

In this chapter, the characteristic of the ship and the design of the permanent magnet synchronous machine are defined. These are included the initial data of the ship, electric constraints of the machines, machines geometry, the material used in the simulation and thermal setting for the machine.

3.1 Operation and Characteristic of the Ship

The Permanent Magnet Synchronous Motor will be implemented in a pod propulsion system for a ship operating between Gothenburg Port and Frederikshavn Port in Denmark. The journey will take approximately 3 hours and 30 minutes with a distance of around 100 km, as shown in Fig. 3.1.

During the journey, the machine will operate at varying speeds, as illustrated in the speed-time profile in Fig. 3.2. In the first 20 minutes, the ship will move at low speed, from 0 km/h to 5.54 km/h, allowing a gradual increase in speed as the ship departs the harbor. From minute 20 to minute 80, the ship's speed will increase to a moderate speed, 12.93 km/h, as the ship navigates through the small islands around Gothenburg. Then, out of the open sea, the ship will reach its full operating speed at 27.80 km/h, from minute 80 to minute 185, representing the longest phase of the journey, where the ship will be running at maximum speed. As the ship approaches Frederikshavn, the speed of the ship will gradually decrease from minute 185, following a controlled deceleration until the ship arrives at a complete stop upon docking at the destination.

Figure 3.1: Route of the ship from Gothenburg harbor in Sweden to Frederikshavn harbor in Denmark

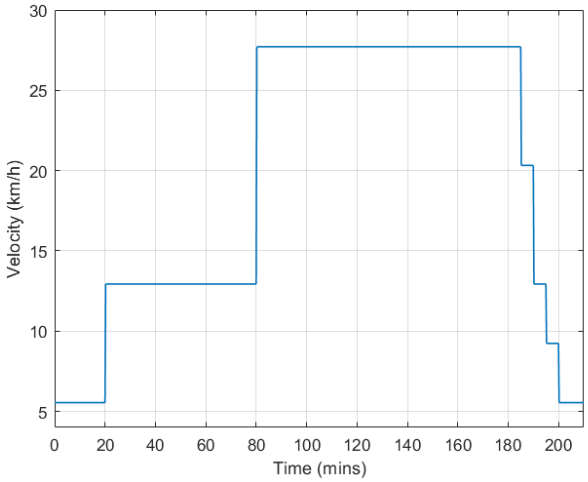

Figure 3.2: Duty cycle of the machine to represent the speed operation of the ship

3.1.1 Characteristic of the ship for the propulsion system

Table 3.1 provides the data on the characteristics of the ship operating between the Gothenburg ports in Sweden and Frederikshavn in Denmark. These data include the weight of the empty ship, the density of the seawater, the wetted surface area, frictional drag coefficient, and propeller radius. The heavier the ship, the larger the wetted surface area will be which defines the frictional resistance.

The ship's wetted surface area, 11150 m^2, represents the contact area between the ship and the seawater. This area affects the amount of friction the ship faces as it moves. The larger the wetted surface area, the greater the friction that must be overcome. The Reynolds number has to be firstly calculated by using (2.3),

$$R_e = \frac{v_{ship}\ L_{WL}}{\nu} = \frac{7.79 \times 300}{1.04 \times 10^{-6}} = 2.24 \times 10^9$$

Next, the coefficient of frictional resistance (C_f) of the ship can be obtained by using (2.2), in which is a multiplier for calculating the frictional resistance between the ship's surface and the seawater,

$$C_f = \frac{0.075}{(\log_{10}(R_e) - 2)^2} = \frac{0.075}{(\log_{10}(2.24 \times 10^9) - 2)^2} \approx 0.0014$$

Then, the friction resistance is obtained by using (2.1),

$$F_{ship} = \frac{1}{2}\rho_{water} S C_f v_{ship}^2 = \frac{1}{2} \times 1025\ \text{kg/m}^3 \times 11150\ \text{m}^2 \times 0.0014 \times 7.79^2\ \text{m/s} = 481\ \text{kN}$$

This resistance will affect the amount of power required to maintain the desired speed of the ship.

Table 3.1: Parameters of the ship

	Variable	Value
Length at waterline	L_{WL}	300 meters
Sea water density	ρ_{water}	1025 kg/m^3
Wetted-surface area	S	11150 m^2
Frictional resistance coefficient	C_f	0.0014
Ship Force	F_{ship}	481 kN
Power	P	3 MW

Fig. 3.3 presents the force of the ship. The total resistance is primarily composed of frictional resistance. The resistance or force grows quadratically with velocity, as indicated by the gradual increase in both force and torque in the graphs. The force increases sharply as velocity increases, following a quadratic relationship due to the dependence of frictional resistance on the ship's speed.

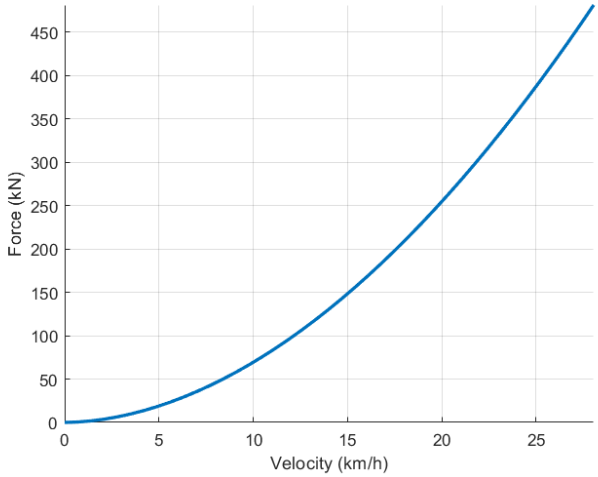

Figure 3.3: Ship force characteristic

Fig 3.4 presents how the power of the ship increases with velocity. This trend follows the increasing of resistance forces quadratically with speed. At lower velocities, the required power is minimal because the resistance forces are relatively small. However, as the velocity increases, the power required to overcome these forces rises significantly. Here, In this ship, the efficiency of the propeller is assumed of 80%. This power is defined by using (2.4) and (2.5),

$$P = F_{ship}\ v_{ship} = 481 \text{ kN} \times 7.79 \text{ m/s} = 3.74 \text{ MW}$$

$$P_{shaft} = P\ \eta_{propeller} = 3.74 \text{ MW} \times 0.8 = 3 \text{ MW}$$

Then, the power to drive the ship forward is 3 MW. From the figure, it can be seen that the increasing power of the ship can increase the energy demand of the ship as it moves through water at higher speeds. This highlights the efficiency challenges faced at higher operating speeds.

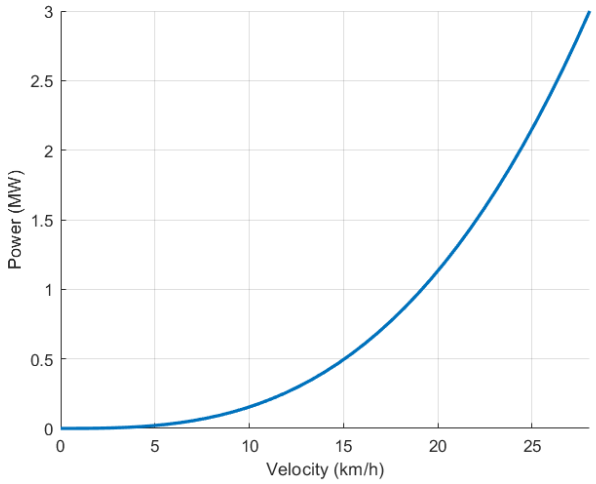

Figure 3.4: Characteristic of the ship power

3.2 Configuration and components of pod propulsion systems

In pod propulsion systems, the electrical setup typically includes components such as a power plant, switchboards, transformers, frequency converters, and propulsion motors. For this discussion, the transformer, frequency converter, and propulsion motor will collectively be referred to as the electrical system, as the power plant and switchboards fall outside the defined scope. Within the ship, the transformer and converter are located in the pod room, while the machines are housed inside the pod. Electrical power is transferred from the converter to the rotating pod using a slip ring. Figure 3.5[14] illustrates a simplified single-line diagram of such a system. Generally, these systems are designed with two pods, each functioning independently but configured identically.

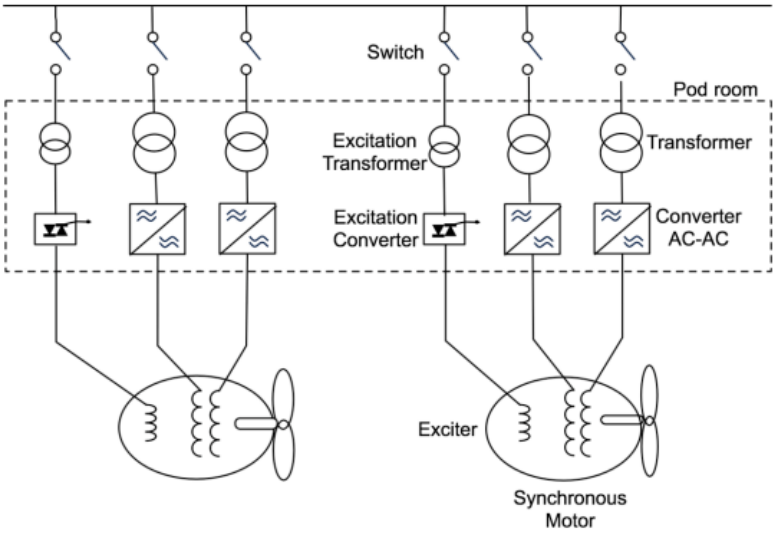

Figure 3.5: The electrical configuration of pod propulsion system

From this configuration, it can be seen that there are two machines in the ship and each of the machines to be designed can generate the power of 1.5 MW. Then, the total power of the machine is around 3 MW.

3.3 Electric Constraints

In this report, the voltage and current supply given to the machines on the electric ship depend on the battery and inverter models used, although these components are not specifically modeled here. The propulsion system for electric ships generally uses a high DC voltage. Therefore, the DC bus voltage in this machine is set at 2200 Volts, and the line-to-line supply voltage then becomes 1556 Volts,rms through (2.20), (2.21) and (2.22),

$$V_{\text{line,rms}} = \frac{\sqrt{3}V_{\text{dc}}}{\sqrt{3}\sqrt{2}} = \frac{2200}{\sqrt{2}} \approx 1556\,\text{Volts,rms}$$

Now, the shaft of ship power is obtained of 3 MW. This ship has two machines to drive during the operation. It can be assumed that each of the machines will supply the power of 1.5 MW. Then, $cos\phi$ is assumed of 0.7. Finally, the maximum current rms can be calculated by using (2.23),

$$I_{max,rms} = \frac{P_{shaft}}{\sqrt{3}\ V_{\text{line,rms}} \cos\phi} = \frac{1.5 \times 10^6}{\sqrt{3} \times 1556 \times 0.7} \approx 800\,\text{Amps,rms}$$

3.4 Parameters of the machine

The synchronous speed is inversely proportional to the number of poles. It means that machines with more poles will have a lower synchronous speed compared to

machines with fewer poles, assuming the frequency of the power supply remains constant. As a stated hypothesis, the machines are designed to rotate at a speed of 75 RPM. Then the initial parameters are assumed and calculated by using (2.24),

$$n_s = \frac{120f}{N_p} = \frac{120 \times 20}{32} = \frac{2400}{32} = 75\,\text{rpm}$$

Here, it can be seen that the machine will be operated at frequency of 20 (Hz) and the number of poles of 32.

Additionally, we assume that the motor has 2 slots per pole per phase, as this allows the motor to have a distributed winding configuration, resulting in a more direct and symmetrical winding within the stator slots. This helps balance the magnetic field and reduce the harmonic content in the motor output, resulting in smoother torque. Combined with the three-phase system (m), the total number of slots (Q_s) can be calculated as 192 by using (2.25),

$$Q_s = q \times N_p \times m = 2 \times 32 \times 3 = 192$$

Thus, Table 3.2 summarizes an original guess of the design parameters of the Neodymium and Ferrite machine to be applied in the simulation.

Table 3.2: Table of the parameters for the permanent magnet synchronous machine

Parameter	Value	Unit
Number of slots	192	-
Number of poles	32	-
Number of pole pairs	16	-
Number of phases	3	-
Number of slots per pole per phase	2	-
Shaft speed	75	RPM
Frequency	20	Hz

3.5 Geometry of the motor

In this report, there are two designs of permanent magnet synchronous motors to be analyzed. The first design uses the Neodymium magnet material and the second design uses the Ferrite magnet material.

Table 3.3 below shows the radial dimensions of the stator and rotor for both motor designs in Motor-Cad. From the table, we assume that both machines have similar dimensions, in which the diameter of the outer stator is 2100 mm, the diameter of the inner stator is 1890 mm, and the length of the air gap is 8 mm.

Table 3.3: Data Geometry of stator and rotor used in MotorCad

Stator	Value	Rotor	Value
Stator outer diameter	2100 mm	Rotor outer diameter	1874 mm
Stator inner diameter	1890 mm	Rotor inner diameter	1000 mm
Slot width	23 mm	Magnet thickness	40 mm
Slot depth	86 mm	Magnet width	60 mm
Stator tooth tip depth	4 mm	Airgap	8 mm

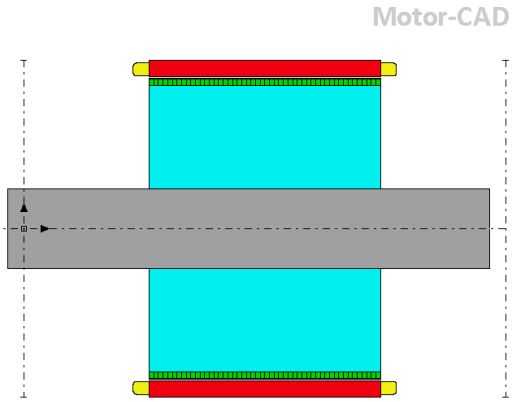

Figure 3.6: Axial motor for the Neodymium machine

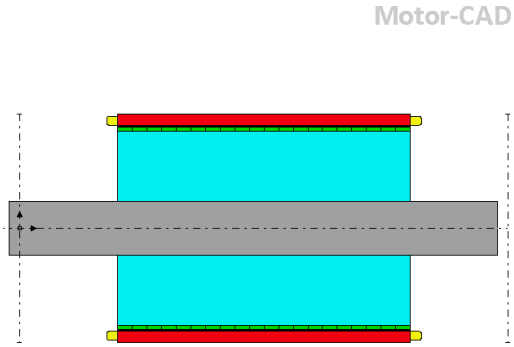

Figure 3.7: Axial motor for Ferrite machine

Fig. 3.6 and 3.7 present the axial motor of the Neodymium and Ferrite machine. The difference between the two designs is in the length of the motor, in which the Neodymium machine has more compact dimensions compared to the Ferrite machine. As an initial guess, the Neodymium machine is 1440 mm long, compared to the Ferrite machine which is 2700 mm long.

3.6 The material selection

Table 3.4and 3.5 are the materials used for the various components of the machines. The material of the stator and rotor for both machines is M800-50A (Silicon steel). The resistivity of M800-50A is much higher than that of conductive materials such as copper. This higher resistivity helps to reduce the eddy currents induced in the material when exposed to alternating magnetic fields, thereby reducing heat losses due to eddy current losses.

The armature winding uses copper, which is the most commonly used material due to its excellent conductivity. It has a low resistivity of 1.72E-08 $Ohm.m$, which can effectively minimize energy losses in the form of heat. Copper also has a temperature coefficient of resistivity of 0.00393 indicating the resistance increases with

temperature. Although resistance changes with temperature, copper's predictable thermal behavior ensures stable performance under various operating conditions.

Table 3.4: Material selection for the Neodymium machine

Component	Material	Specification
Stator	M800-50A	Appendix A.1
Winding	Copper	Appendix A.2
Rotor	M800-50A	Appendix A.1
Shaft	Milled Steel	Appendix A.3
Magnet	Neodymium (N30UH)	Appendix A.4

Table 3.5: Material selection for the Ferrite machine

Component	Material	Specification
Stator	M800-50A	Appendix A.1
Winding	Copper	Appendix A.2
Rotor	M800-50A	Appendix A.1
Shaft	Milled Steel	Appendix A.3
Magnet	Ferrite (Y34)	Appendix A.5

Moreover, different magnet materials, N30UH for the Neodymium machine and Y34 for the Ferrite machine, are used for comparative analysis. Figs. 3.8 and 3.9 are the characteristics of the demagnetization curve of the materials. When the temperature is 20 °C, the Neodymium magnet has a higher remanent flux density of 1.125 $Tesla$ and a higher coercive force of 1990 kA/m compared to the Ferrite magnet, which has a remanent flux density of 0.43 $Tesla$ and a coercive force of 220 kA/m. This means that the Neodymium can maintain a stronger magnetic field and resist demagnetization more effectively under the same temperature. Therefore, this report will analyze and compare the Neodymium and the Ferrite as magnet materials to identify the most suitable solution for the motor out of these options.

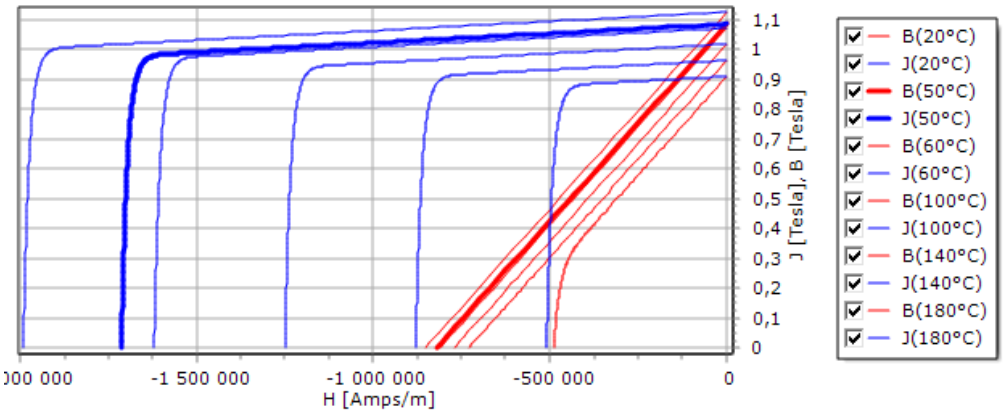

Figure 3.8: Demanetization curve characteristic of Neodymium magnet

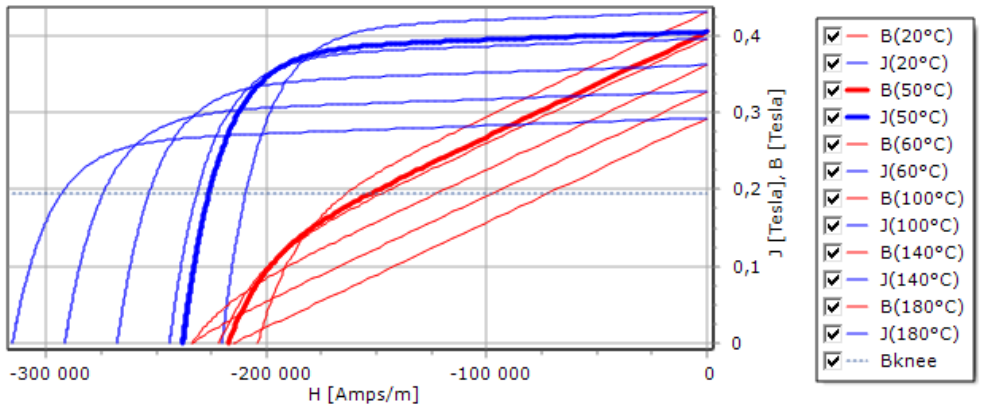

Figure 3.9: Demagnetization curve characteristic of Ferrite magnet

3.7 Thermal and cooling setting

Fig. 3.10 shows the thermal model and related parameters of the motor and the machine using a submersible cooling system. As mentioned before, The submersible cooling method achieves efficient thermal management by completely immersing the motor in seawater, allowing for direct heat dissipation from the motor components to the surrounding environment. This method significantly enhances cooling efficiency, as seawater can absorb heat more effectively than air. This ensures the design in a combination of motor and cooling media can prevent overheating under high load conditions [8].

The primary heat sources in the machines are the copper losses generated by the windings and the iron losses from the magnetic core. The submersible cooling method facilitates direct contact between the sea and the machines housing, promoting efficient heat transfer away from the machines. By reducing the temperature rise associated with both copper and iron losses, this cooling prevents damage to machines components and extends machines life by reducing the temperature rise associated with copper and iron losses.

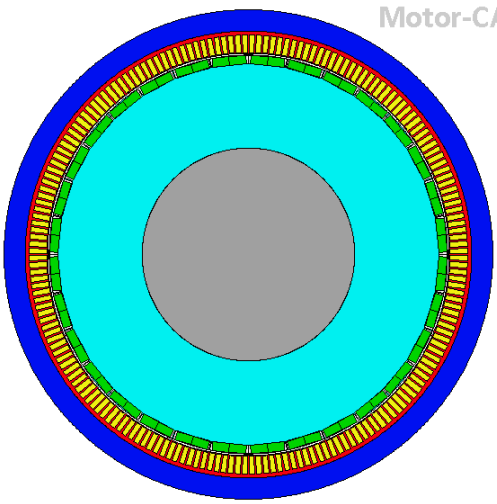

Figure 3.10: The machine thermal model in the Motorcad

Table 3.6 [15] and Table 3.7 [16] show the temperature levels of magnets and insulation materials in the machines. These temperature levels help us determine the tolerance of magnets and insulation materials in different working environments. If the temperature is too high, the magnetic force will be weakened, the magnet can be damaged, and the insulation material may lose its insulation performance due to overheating. Therefore, in the motor temperature simulation process, to provide a sufficient temperature margin, we chose the magnet temperature class UH and insulation class H as our measurement standards.

Table 3.6: Table of the magnet temperature classes

Magnet temperature class	N	M	H	SH	UH	EH
T°C	80	100	120	150	180	200

Table 3.7: Table of the Insulation classes

Insulation class	A	B	F	H
T°C	105	130	155	180

Table 3.8 provides critical data regarding the external fluid properties of a submersible cooling system, which plays a crucial role in thermal management. The table highlights several physical and thermal properties of the fluid, starting with thermal conductivity indicating the fluid's ability to transfer heat, a vital factor in the cooling system's efficiency. The density of the fluid reflects its mass per unit volume, which influences the fluid's inertia and flow behavior.

The fluid's specific heat capacity (C_p) shows its ability to store heat energy per unit mass. This is an essential parameter for understanding how much heat the fluid can absorb while undergoing a temperature change. The kinematic viscosity

measures the fluid's resistance to flow under gravitational forces and is derived from the dynamic viscosity divided by density.

The volumetric expansion coefficient quantifies how the fluid's volume changes with temperature, affecting its buoyancy-driven flow in natural convection. Lastly, the dynamic viscosity measures the fluid's internal resistance to flow, directly impacting the energy required to pump the fluid through the cooling system.

Table 3.8: Data of the submersible cooling system

External fluid data	Value
Thermal conductivity	0.59 $W/(m \cdot K)$
Density	998.10 kg/m^3
Specific heat capacity (C_p)	4182 $J/(kg \cdot K)$
Kinematic Viscosity	9.94E-7 m^2/s
Volumetric expansion coefficient	21.2E-5 1/K
Dynamic viscosity	99.2E-5 $Pa \cdot s$

4

Analysis

This chapter mainly shows the simulation results of the machine's performance regarding the electromagnetic, winding, flux density, temperature, losses and efficiency, drive cycle, mechanical, and environmental impact of the Neodymium and the Ferrite machine.

4.1 The machine electromagnetic simulation results

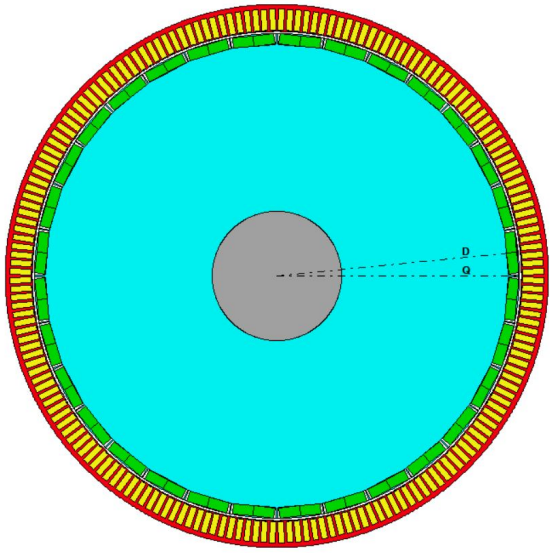

Figure 4.1: Radial machine model

Fig. 4.1 shows the radial model of the machine used in the simulation. First, the power of one machine is around 1.5 MW, but in the ship, there are two machines of the same power working in two pods, so it can be concluded that the two machines can produce power about 3 MW of power for propulsion. Then as can be seen from the Table 4.1, the output power of the machines are not much different. Still, the input power of the Ferrite machine is slightly higher than that of the Neodymium machine, which shows that the Ferrite machine has a higher energy demand when achieving similar output. In addition, the average torque of the Ferrite machine is higher than that of the Neodymium machine, indicating that the Ferrite machine can provide higher mechanical output under the same conditions.

Secondly, the loss of the Ferrite machine is much higher than that of the Neodymium machine, and the difference in their losses in material design is particularly obvious, which we will be analyzed in detail in subsequent chapters. The higher loss of the Ferrite machine will lead to a decrease in its efficiency. The system efficiency of the Ferrite machine is 94.1%, and that of the Neodymium machine is 95.9%, with a difference of 1.8%. This shows that the priority of the Neodymium machine as a material selection for ships is higher than that of the Ferrite machine because from the perspective of energy costs and long-term navigation, losses and efficiency should be the first considerations for the ships.

Table 4.1: The simulation results of the machines

Variable	The Neodymium machine	The Ferrite machine
Input Power	1565 kW	1613 kW
Total Losses	64.19 kW	95.34 kW
Output Power	1500 kW	1517 kW
Machine Efficiency	95.9%	94.1%

4.2 The winding of the machine

As a first guess, we assumed the winding of these machines to be as seen in Fig. 4.2. The slot type used in the machines was designed as a rectangular form, and the wire type is also rectangular. This rectangular form will give a higher fill factor compared to a round winding.

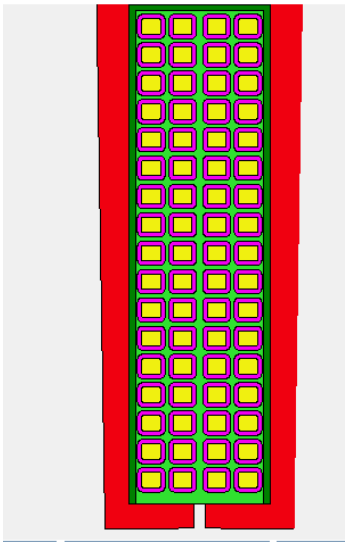

Figure 4.2: Figure of the winding set of the machines

Table 3.3 provides the data to calculate the area of the slot in the machines. This slot has a width of 23 mm and depth of 86 mm. Then, this data and (2.26) can be used to determine the area of the winding slot,

$$A_{slot} = 23\text{mm} \times (86 - 4)\text{mm} = 1886 \text{ mm}^2$$

Besides, the rectangular conductor area can be calculated by using (2.27),

$$A_{cond} = (3 + 1.4)(2.5 + 1.4) - 4 \times 0.7^2 + \pi \times 0.7^2 \approx 16.7 \text{ mm}^2$$

Finally, we can get the number of conductors per slot, which can be calculated by (2.28),

$$N_{cond} = \frac{1886 \text{ mm}}{16.7 \text{ mm}^2} \times 0.65 \approx 68$$

This winding design has a slot fill factor (with insulation) of 65%. However, the fill factor without insulation is lower at 30%. It is because the thickness of the conductor insulation is quite thick, namely at 0.7 mm. Generally, the fill factor generally refers to the ratio of the actual conducting material area filled in the stator slot to the total effective volume of the slot. Then, a reasonable the fill factor rate is usually between 40% and 60%, which can ensure that the machines can provide sufficient heat dissipation space[17].

Table 4.2 shows the winding parameters obtained from the previous equations. These machines have a slot area of 1886 mm^2, a conductor area of 16.7 mm^2, and the number of conductors that can be filled per slot is 68 wires. Moreover, the machines adopt a double-layer winding.

Table 4.2: The winding parameters

Parameter	Value
Conductor width (W_{cond})	3 mm
Conductor height (L_{cond})	2.5 mm
Insulation thickness (r)	0.7 mm
Fill factor with insulation (k_{fill})	65 %
Fill factor without insulation (k_{fill})	30 %
Slot area (A_{slot})	1886 mm^2
Single conductor area without insulation (A_{cond})	7.5 mm^2
Single conductor area with insulation (A_{cond})	16.7 mm^2
Number of conductors per slot (N_{cond})	68
Number of conductor strands (N_{strand})	34

To calculate the winding resistances, the length of the winding used on the machines must be known first. By using (2.30), the end winding turn length of the conductor for both machines can be calculated by,

$$l_{EW} = 1.2\frac{\pi \times 1890 \text{ mm}}{32} \approx 223\,\text{mm}$$

Then, through the (2.29) , total turn length can be obtained by,

$$l_{\text{turn, Neodymium}} = 2 \times (1440 \text{ mm} + 223 \text{ mm}) \times 68 \approx 226\,\text{m}$$

$$l_{\text{turn, Ferrite}} = 2 \times (2700 \text{ mm} + 223 \text{ mm}) \times 68 \approx 397\,\text{m}$$

Here, the stator winding for both machines were simulated in 120°C, then the conductor resistivity can be calculated by using (2.34),

$$\rho(T) = 1.72 \times 10^{-8} \times [1 + 0,00393 \times (120 - 20)] = 2.42 \times 10^{-8} \text{ Ohm.m}$$

The total area of the conductor used can be obtained by multiplying the single conductor area without insulation by the number of conductor strands. Then, (2.33) on Section 2.4.1 is used to obtain the resistances of both machines.

$$R_{\text{Neodymium}} = \frac{2.42 \times 10^{-8} \text{ Ohm.m} \times 226 \text{ m}}{7.5 \text{ mm}^2 \times 34} \approx 0.020 \text{ Ohms}$$

$$R_{\text{Ferrite}} = \frac{2.42 \times 10^{-8} \text{ Ohm.m} \times 397 \text{ m}}{7.5 \text{ mm}^2 \times \ 34} \approx 0.042 \text{ Ohms}$$

Tab 4.3 summarizes that the length of the wire for the Ferrite machine is longer compared to the Neodymium machine because the active turn length of the Ferrite machine is longer. This results in higher resistance on the Ferrite machine than on the Neodymium machine and can affect losses on both machines.

Table 4.3: Length and resistance per phase of the wire for both machines

Parameter	**Neodymium Machine**	**Ferrite Machine**
Active winding turn length	1440 mm	2700 mm
End winding turn length	223 mm	223 mm
Total turn length of the winding	226 meters	397 meters
Resistance	0.020 Ohms	0.042 Ohms

Finally, the machines have obtained the current density of 3.14 Amps/mm^2 by using (2.31),

$$J = \frac{800 \text{ Amps,rms}}{7.5 \text{ mm}^2 \times 34} \approx 3.14\,\text{Amps/mm}^2$$

4.3 Flux density of the machines

Fig. 4.3 and 4.4 are the flux density obtained by the machines and Table 4.4 shows more accurate flux density data.

The flux density of the air gap, stator teeth, stator back iron, and rotor back iron in the Neodymium machine are generally higher and more uniform. The peak value of the stator tooth tip flux density in the Neodymium machine is 2.3 T, while the peak value of the Ferrite machine is 1.9 T. This higher value indicates that the use of the Neodymium magnet can support a stronger and more concentrated magnetic field. The airgap Flux Density in the Neodymium machine is 0.85 Tesla and 0.48 Tesla for the Ferrite machine.

This simulation result shows that the design of the machines is effective in utilizing both magnet materials because the ideal airgap flux density is 0.7-1.5 Tesla. The Ferrite machine only reaches about 0.4 Tesla. In addition, it can be seen from Fig. 3.8 and 3.9 that the remanence and coercive force of the Neodymium magnet are significantly higher than those of the Ferrite magnet under the same conditions, which means that it can create a stronger magnetic field for the same volume. In terms of ship propulsion, it will provide higher efficiency and torque.

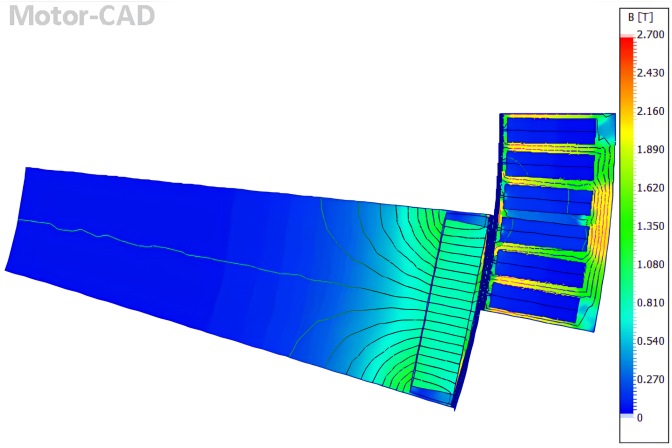

Figure 4.3: The flux density figure of Neodymium machine

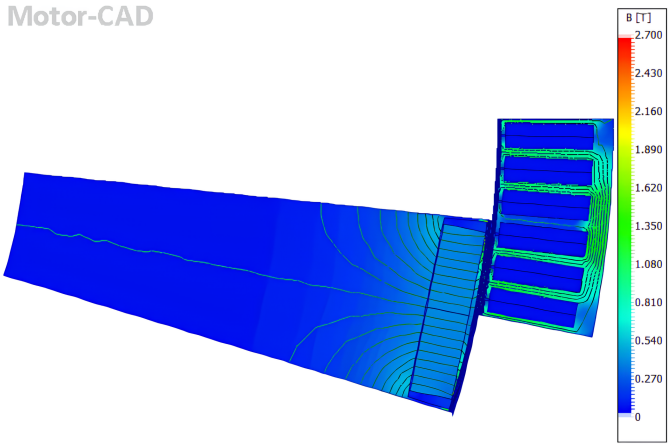

Figure 4.4: The flux density figure of Ferrite machine

Table 4.4: The result of the flux density

Variable	Neodymium machine	Ferrite machine
Airgap Flux Density	0.85 Tesla	0.48 Tesla
Stator Tooth Flux Density	2.00 Tesla	1.55 Tesla
Stator Tooth Tip Flux Density	2.30 Tesla	1.90 Tesla
Stator Back Iron Flux Density	2.14 Tesla	1.48 Tesla
Rotor Back Iron Flux Density	0.03 Tesla	0.01 Tesla

The Neodymium and the Ferrite machines have been assessed under a demagnetization testing condition to evaluate their safety operational limits, specifically by setting the phase angle to set the I_d to $-I_{max,rms}$, which is -800 Amps,rms. This setup is critical to understanding the machines' magnetic flux behavior under high-

stress conditions that may approach or exceed the limits of safe operation. Table 4.5 presents the results for both machines.

In this test, the flux density of the machines is slightly reduced compared to their magnetization condition. For instance, the airgap flux density in the Neodymium machine is 0.75 Tesla, whereas, in the Ferrite machine, it is only 0.31 Tesla. Similar reductions are observed in other areas, indicating that both machines operate in a weakened magnetic state when subjected to this negative direct-axis current.

This reduction in flux density reflects the machines' operation within a critical, near demagnetization zone, where the magnetic material's ability to sustain high flux density is compromised. The Neodymium machine, with higher peak flux densities across all regions compared to the Ferrite machine, demonstrates a superior tolerance towards demagnetization. However, even with Neodymium, this condition should be carefully managed.

To ensure reliable performance and longevity, it is crucial to avoid this extreme operating condition. Keeping I_d within safe positive values rather than at $-I_{max,rms}$ could help maintain the sufficient flux densities and prevent the machine from entering the demagnetization zone.

Table 4.5: The result of the flux density in demagnetization testing condition

Variable	Neodymium machine	Ferrite machine
Airgap Flux Density	0.75 Tesla	0.31 Tesla
Stator Tooth Flux Density	1.66 Tesla	0.71 Tesla
Stator Tooth Tip Flux Density	2.26 Tesla	1.94 Tesla
Stator Back Iron Flux Density	1.84 Tesla	0.23 Tesla
Rotor Back Iron Flux Density	0.025 Tesla	0.008 Tesla

4.4 Torque-speed plot and MTPA trajectory

Figure. 4.5 shows the torque performance of the machine. In this graph, the maximum torque of the machine at a maximum speed of 75 RPM is approximately 195 kNm, which can be obtained using (2.13), which corresponds to the end-of-curve value. This torque is essential for large ships to overcome initial resistance and maintain steady acceleration at lower speeds.

$$T_e = \frac{P_e}{\Omega_r} = \frac{1.5 \text{ MW}}{75 \text{ RPM } \frac{\pi}{30}} = 190.9 \text{ kNm}$$

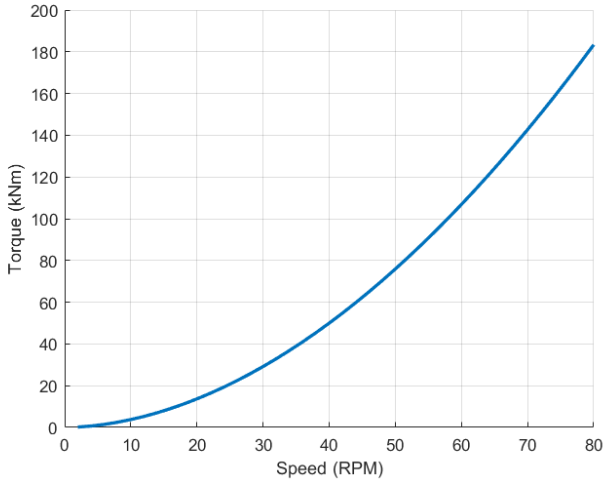

Figure 4.5: Torque-speed plot characteristic of the machine

The MTPA (Maximum Torque Per Ampere) curve in the i_d and i_q axis represents the optimal current trajectory for achieving maximum torque per unit of the current. This refers to Section 2.2.2. The curve is typically located in the negative i_d region and positive i_q region, reflecting the machine's operational strategy to balance torque production and field weakening. Specifically, i_q is primarily responsible for torque generation, while i_d influences the magnetic field's strength and provides field-weakening functionality. The plot indicates that as i_q increases, i_d becomes increasingly negative, which is characteristic of optimal current control for machines operating under MTPA.

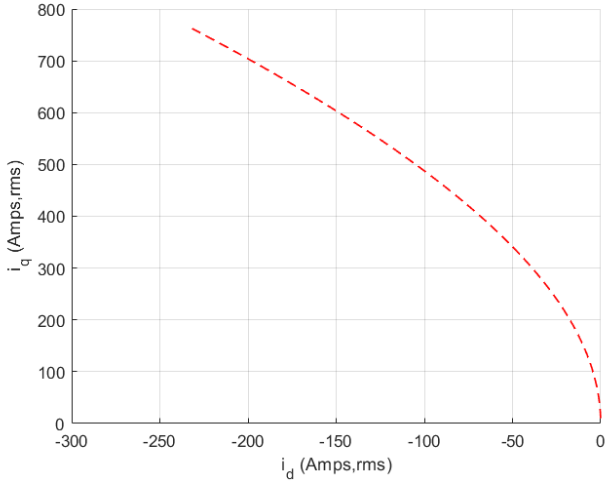

Figure 4.6: The MTPA plot of the machines

4.5 Temperature of the Machines

Fig. 4.7 and 4.8 are the temperature distributions of the Neodymium and the Ferrite machines, respectively. We assume that the seawater temperature is 21 degrees.

Table 4.6 shows the temperatures of different parts of the machine.

The motor housing temperature is 30°C, indicating that the seawater immersion cooling system effectively removes the heat generated inside the machines. The magnet temperatures are 62°C and 63°C respectively. According to the magnet grades in Table 3.6, the magnet temperatures are much lower than the UH maximum operating temperature of 180°C, so it can be judged that the magnet part is well-designed [15].

Secondly, the average winding temperature of the Neodymium machine is 106°C, and the average winding temperature of the Ferrite machine is 89°C. According to the winding insulation level in Table 3.7, the insulation level of the stator winding can usually withstand higher temperatures (such as 130°C, 155°C, and 180°C), and compare with our assumption, the temperature of insulation level is lower than the H class(180℃) so the winding temperature in both cases is very safe[16]. In contrast, the Neodymium machine has a higher performance but will produce a higher average winding temperature, indicating greater power loss in the winding or greater heat dissipation challenges.

In addition, the rotor yoke temperature of the two materials shows similar values, with the Ferrite machine being slightly higher, 62°C, while the rotor yoke temperature of the Neodymium machine is 60°C, indicating that the Ferrite machine transfers more heat to the rotor yoke than the Neodymium machine. In addition, the stator yoke of the Ferrite machine runs warmer, 79°C, than the Neodymium machine, 65°C. This indicates that the stator of the Ferrite machine is heated more locally due to slightly higher iron losses in the core. The shaft center temperature of the Ferrite machine at 56°C is slightly higher than that of the Neodymium machine at 51°C. This indicates that the rotor and shaft assembly of the Ferrite machine accumulates more heat, which may affect the bearing system or mechanical integrity if not adequately cooled.

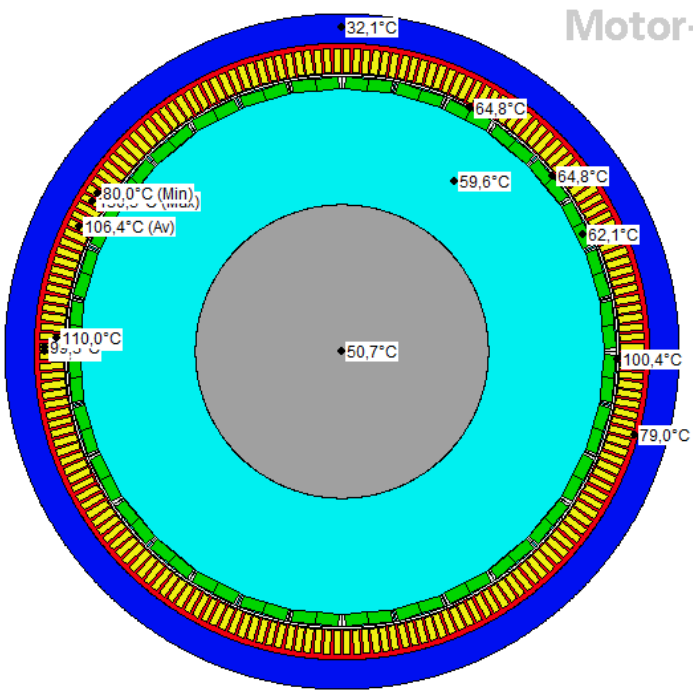

Figure 4.7: The temperature distribution figure of the Neodymium machine

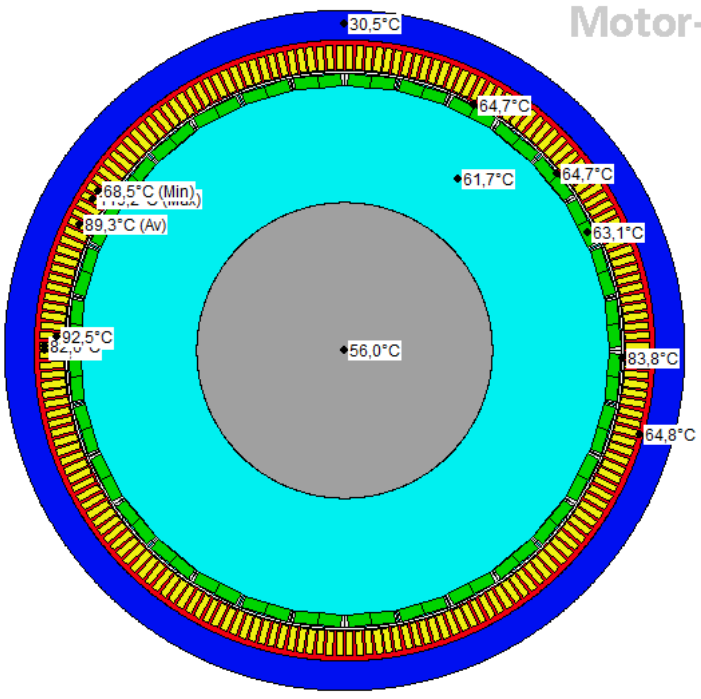

Figure 4.8: The temperature distribution figure of the Ferrite machine

Table 4.6: The temperature distribution for different conditions.

Machine Part	Neodymium machine	Ferrite machine
Housing	32 ℃	31 ℃
Magnet	62 ℃	63 ℃
Magnet pole	65 ℃	65 ℃
Rotor surface	65 ℃	65 ℃
Rotor yoke	60 ℃	62 ℃
Shaft center	51 ℃	56 ℃
Stator yoke	65 ℃	79 ℃
Winding	106 ℃	89 ℃

4.6 Losses and Efficiency of the Machines

4.6.1 Losses of the machines

Fig. 4.9 and 4.10 present iron losses for the Neodymium and the Ferrite machines, respectively. The maps show a clear relationship where speed is the dominant factor affecting the iron losses, while torque has a minimal impact. As speed increases, iron losses rise significantly, even when the torque remains constant. For example in the Neodymium machine, when the machine is operating at speed of 50 RPM and 100 kNm of torque, the iron loss shows around 14.87 kW, but it increases sharply to about 23.86 kW at 75 RPM of speed and 190 kNm of torque. This trend is consistent across all torque levels, showing that torque has little effect on iron losses and indicating that iron losses are primarily driven by the electrical frequency, which is directly proportional to speed, based on (2.35) and (2.36).

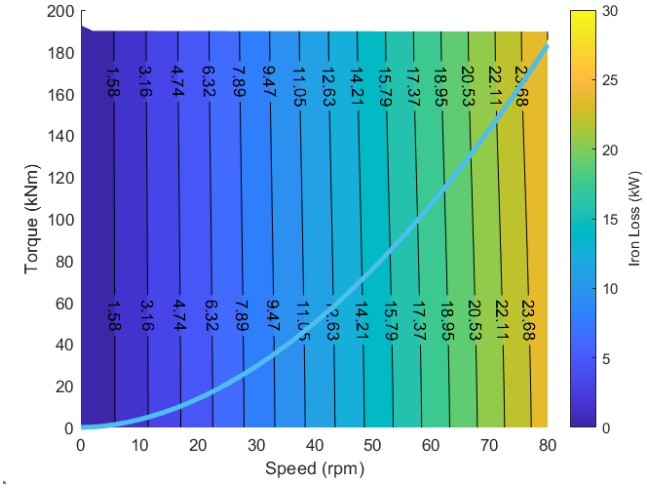

Figure 4.9: Iron loss characteristics in Neodymium machine

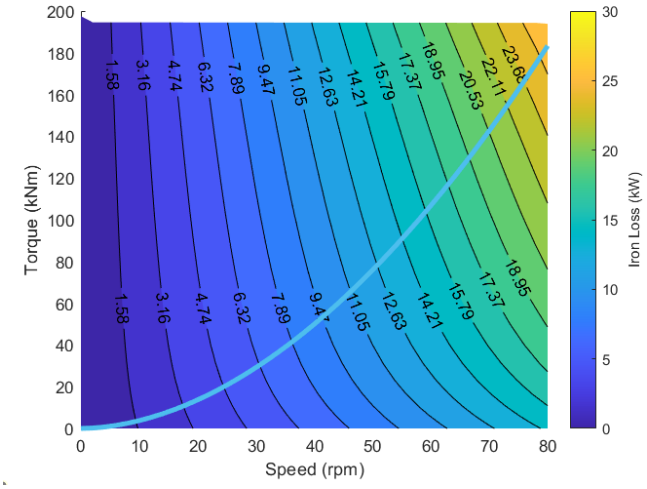

Figure 4.10: Iron loss characteristics in Ferrite machine

Table 4.7 shows the losses in the Neodymium and the Ferrite machine when both machines are operating at maximum speed, 75 RPM, and torque, around 200 kNm. Firstly, it can be seen from the table that the stator copper loss of the Neodymium machine is 40.66 kW and the copper loss of the Ferrite machine is 69.85 kW indicating that the Neodymium machine produces lower losses than the Ferrite machine, less heat generated in the armature, and higher efficiency.

The stator and rotor iron loss produced by the two machines are very similar. Iron losses include hysteresis losses and eddy current losses. These losses are more closely related to the machine's material and design than the winding material, which indicates that the performance in this regard is comparable [18]. The stator iron loss produced by the Neodymium machines is 23.36 kW, slightly lower than those of the Ferrite machine at 25.26 kW, indicating better performance in reducing iron losses caused by the flux. The reduced stator loss of the Neodymium machine further

improve the overall efficiency.

The Neodymium machine ends up with total losses of 64.19 kW, which is lower than 95.34 kW of the Ferrite machine, making the Neodymium magnets a better choice for high-performance applications where energy efficiency and thermal management are critical. In addition, the mechanical losses consisted of friction loss and windage loss were simulated are very low. These losses can be determined by using (2.38) and (2.39). The windage loss in the Neodymium machines is 6.7 Watt, while in the Ferrite machine is 12.5 Watt. Moreover, both of machines have the friction loss at 0.12 Watt. Due to the low value of losses in these mechanical losses, their value are neglected. These types of losses tend to increase significantly only at very high rotational speeds because bearing wear and air resistance are functions of speed. In applications where the machines operate at low to moderate speeds, these losses remain small compared to copper and iron losses.

Table 4.7: Losses of the machines at maximum speed and torque

Variable	Neodymium machine	Ferrite machine
Stator Copper Loss	40.66 kW	69.85 kW
Stator Iron Loss	23.36 kW	25.26 kW
Rotor Iron Loss	0.16 kW	0.23 kW
Total Losses	64.19 kW	95.34 kW

4.6.2 Efficiency of the machines

Figs. 4.11 and 4.12 show the efficiency distribution of the Neodymium and the Ferrite machines under different speed and torque conditions. The Neodymium machine has efficiency of 95.9%, while efficiency of the Ferrite machine is 94.1%. The area with the highest efficiency is concentrated in the high speed and high torque range, indicating that the current path, magnetic flux distribution, and cooling and heat dissipation design of the machines have reached the optimal state, so the efficiency is relatively high. The area with lower efficiency (blue area) appears in the low torque and low-speed range. This is because the fixed losses such as iron loss accounts for a large proportion at low torque.

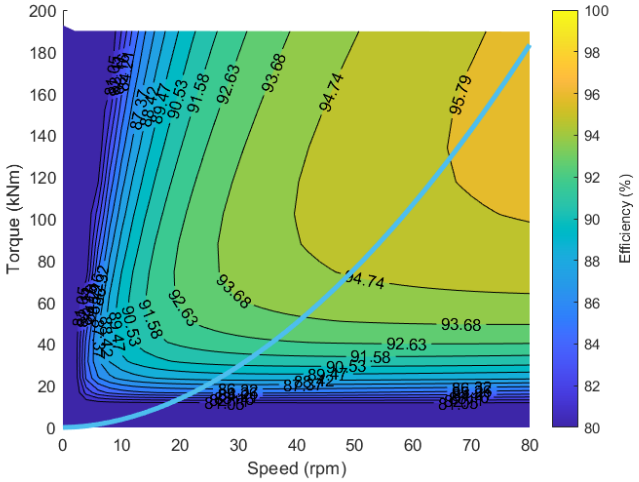

Figure 4.11: The Efficiency map of the Neodymium machine

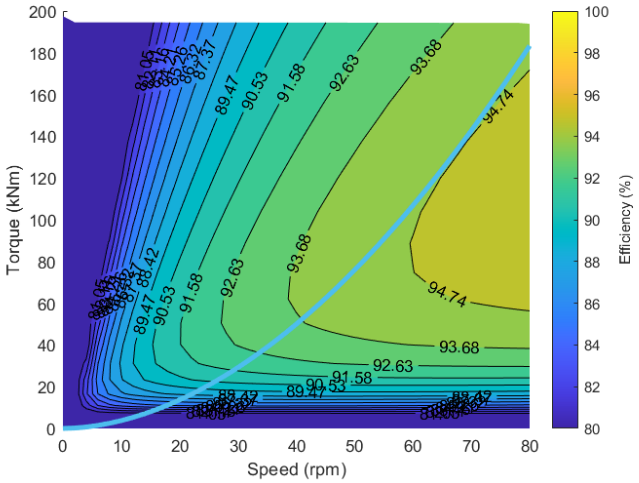

Figure 4.12: The Efficiency map of the Ferrite machine

4.7 Comparison of drive cycle performances of the machines

Fig. 4.13 present the losses in the drive cycle, consisting of total loss of the Neodymium and Ferrite machine. The Neodymium machine indicates a more efficient during the operational. The total losses of the Neodymium machine is lower, 0.18 MWh, compared to the Ferrite machine, 0.24 MWh. This represents the Ferrite machine has a heavier operation profile.

In the 4.6.1 section, the stator copper losses shows more dominant that the iron losses. The increase in the copper loss indicates that it is related to the current supplied to the machines. As a result, the temperature in the windings tends to rise

because the heat generated by these losses cannot dissipate immediately. The elevated temperature in the windings can accelerate insulation degradation and impact component reliability in the long term.

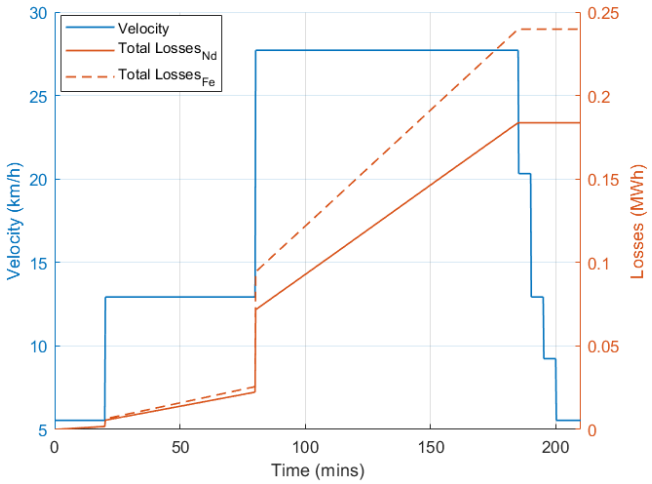

Figure 4.13: Losses comparison in the machines during the drive cycle operation

Fig. 4.14 shows the energy consumption of the Neodymium and the Ferrite machine during the operation. Initially, the ship gradually accelerates from 0 to 80 minutes, and energy consumption increases slowly, reflecting moderate resistive and core losses. Between 80 and 180 minutes, during high-speed cruising, both the Neodymium and the Ferrite machines rise sharply, indicating higher energy demand due to increased winding losses iron losses (eddy and hysteresis losses). After 180 minutes, as the speed reduces, the energy consumption decreases, reflecting reduced load and speed. It indicates that the energy consumption is highest during prolonged high-speed operation, where copper and core losses are elevated. Finally, the energy consumption of both machines has a similar value, where the Neodymium machine is 4.59 MWh, while the energy consumption of the Ferrite machine is 4.68 MWh.

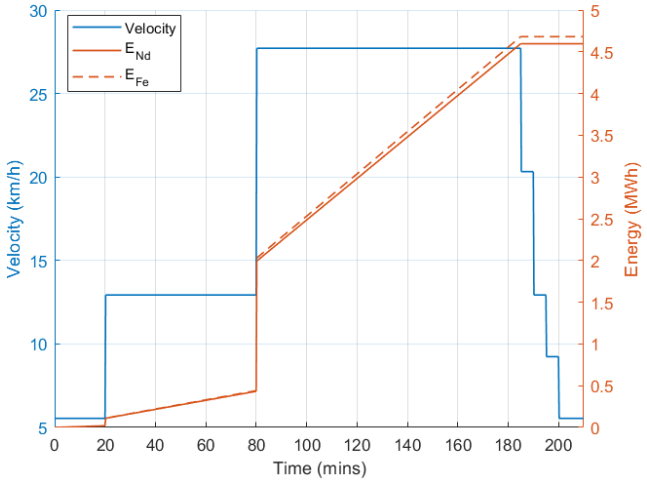

Figure 4.14: Energy consumption for both machines

4.8 Mechanical Simulation of the Machines

A detailed stress analysis of the rotor components was simulated and analyzed, regarding the mechanical stress distribution in the rotor laminations and magnetic bridges under operation conditions, two machines (the Neodymium and the Ferrite). The rotor lamination stress is mainly concentrated in the magnetic bridge area of the rotor, which is the maximum stress caused by the centrifugal force or other mechanical loads in the rotor lamination material. The rotor lamination stress is 87.89 MPa in the Neodymium machine, while the rotor lamination stress is 58.32 MPa in the Ferrite machine. This indicates that the Neodymium machine exerts a greater force in the structure due to its stronger magnetism. The yield stress of the rotor lamination material is 300 MPa, which is the maximum stress that the rotor lamination material can withstand before plastic deformation occurs.

$$\mathrm{SF}_{\mathrm{Neodymium}} = \frac{\sigma_{\mathrm{yield}}}{\sigma_{\mathrm{max}}} = \frac{300\,\mathrm{MPa}}{87.89\,\mathrm{MPa}} \approx 3.41 \tag{4.1}$$

$$\mathrm{SF}_{\mathrm{Ferrite}} = \frac{\sigma_{\mathrm{yield}}}{\sigma_{\mathrm{max}}} = \frac{300\,\mathrm{MPa}}{58.32\,\mathrm{MPa}} \approx 5.14 \tag{4.2}$$

where σ_{yield} is the Rotor Lamination Yield Stress Limit, σ_{max} is the Rotor Lamination Stress (max).

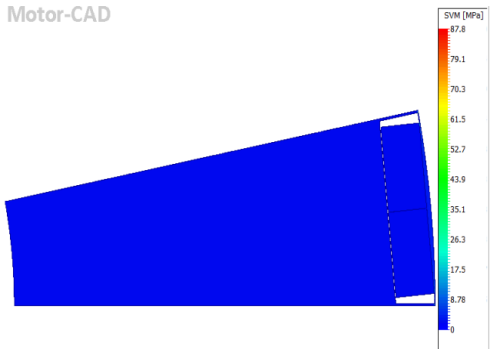

Figure 4.15: The rotor stress of the Neodymium machine

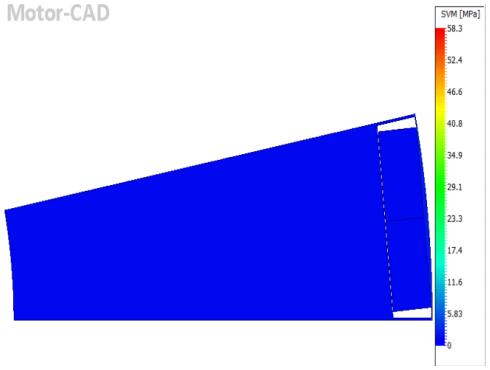

Figure 4.16: The rotor stress of the Ferrite machine

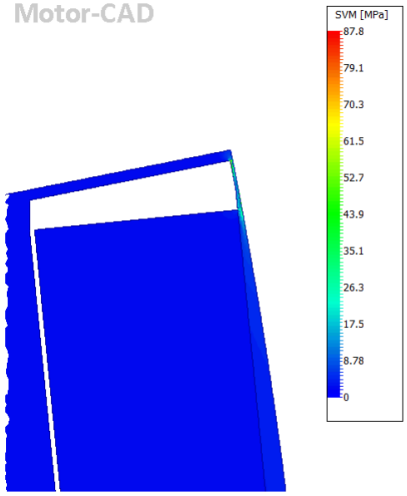

Figure 4.17: The magnetic bridge stress of the Neodymium machine

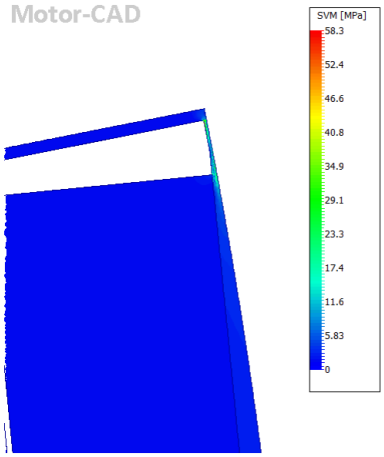

Figure 4.18: The magnetic bridge stress of the Ferrite machine

The safety factor is the ratio of the yield stress of the lamination material to the lamination stress. (4.1) and (4.2), respectively, represent the safety factor ratios for different material applications [18]. The safety factor for the Neodymium machine is 3.41, and the other is 5.14. First, their safety factors are much greater than 1, indicating that the design is safe, that is, the material will not yield under the maximum working stress [18]. Secondly, the safety factor for the Ferrite machine is higher than the Neodymium machine, indicating that although the Neodymium machine can withstand higher stress due to its stronger magnetism, its safety margin is lower than the Ferrite machine.

In addition, stress analysis shows that the calculation of the stress concentration factor (SCF) is also extremely important. Table 4.8 shows that the rotor lamination stress (average) in the Neodymium machine is 0.45 MPa and 0.37 MPa in the Ferrite machine.

$$SCF_{\text{Neodymium}} = \frac{\sigma_{\max}}{\sigma_{\text{ref}}} = \frac{87.89\,\text{MPa}}{0.4499\,\text{MPa}} \approx 195.3 \tag{4.3}$$

$$SCF_{\text{Ferrite}} = \frac{\sigma_{\max}}{\sigma_{\text{ref}}} = \frac{58.32\,\text{MPa}}{0.3681\,\text{MPa}} \approx 158.4 \tag{4.4}$$

where σ_{ref} is the Rotor Lamination Stress (average).

Therefore, the stress concentration factor (SCF) of the two cases can be obtained by (4.3) and (4.4) [19] to be approximately 195 and 158, respectively, which means that in the magnetic bridge area of the rotor, the stress is approximately 195 and 158 times the nominal stress.

Although the rotor design is currently within the safe operating limit, this value is larger than usual, which may lead to potential risks in the magnetic bridge area under long-term operation. Therefore, we can use materials with higher strength or more fatigue resistance than the Neodymium and the Ferrite in this area. These findings emphasize the need to carefully manage stress concentration in high-speed rotors to prevent material fatigue and failure [19]. Moreover, the average stress value of the magnetic bridge part is lower than the yield strength of the Neodymium machine, so the design is also reasonable.

In summary, the simulation results show that the current rotor design is structurally reasonable under operating conditions. However, the determination of high-stress concentration factors in the magnetic bridge suggests that further design optimization may be required to ensure long-term reliability, especially in high-speed applications.

Table 4.8: The stress parameters for different conditions

Variable	Neodymium machine	Ferrite machine
Rotor Lamination Yield Stress limit	300 MPa	300 MPa
Rotor Lamination Stress (average)	0.45 MPa	0.37 MPa
Rotor Lamination Stress (max)	87.89 MPa	58.32 MPa
Rotor Lamination Yield Stress ratio	0.29	0.19
Rotor Lamination Safety Factor	3.41	5.14
Rotor Lamination displacement (average)	0.0015 mm	0.0012 mm
Rotor Lamination displacement (max)	0.024 mm	0.016 mm
Average Magnet Bridge Stress (L1)	42.06 MPa	27.97 MPa

4.9 Environmental impact analysis

Environmental impact refers to the effects of human activities on the natural environment, encompassing changes in the physical, chemical, and biological components

of ecosystems. These impacts are often the result of industrial processes, resource extraction, waste generation, and energy consumption, which contribute to issues such as climate change, biodiversity loss, air and water pollution, soil degradation, and resource depletion. The significance of these impacts is evaluated through various metrics, including environmental footprint analyses and life cycle assessments (LCA), which help quantify the extent of damage to natural systems. Understanding environmental impacts is crucial for developing mitigation strategies, implementing sustainable practices, and guiding policy decisions aimed at reducing the ecological footprint of human activities.

4.9.1 Environmental Priority Strategies (EPS)

Table 4.9 presents a comparison of the environmental impact of both magnet materials for the Neodymium and the Ferrite. This table shows that the Neodymium magnet material has a higher environmental impact compared to the Ferrite material, in which the total impact of the Neodymium magnet is 102.8 $euro/kg$ than 2.9 $euro/kg$ for the Ferrite.

Table 4.9: Comparison of material composition between the Neodymium and Ferrite machine [20][21]

Magnet	**Material Composition**	**Weight (%)**	**ELU (euro/kg)**	**Total impact (euro/kg)**
Neodymium	Neodymium	25.7	202	51.8
	Dysprosium	3.3	1500	49.4
	Iron	69.1	1	0.7
	Boron	1.3	9.1	0.1
	Nickel	0.7	124	0.8
	Total	**100**	**-**	**102.8**
Ferrite	Strontium	3.6	0.2	0.001
	Lanthanum	0.8	175	1.4
	Cobalt	0.3	205	0.7
	Iron	80.9	1	0.8
	Oxygen	14.4	0	0
	Total	**100**	**-**	**2.9**

Moreover, Table 4.10 shows the environmental impact for both machine models, the Neodymium and the Ferrite. As can be seen, the total impact of the Ferrite machine is lower compared to that of the Neodymium machine. In the Neodymium machine,

the biggest environmental impact comes from the use of the magnet contributing to around 227,393 *euro* and Copper as a winding, which is around 200,823 *euro*. For the Ferrite machine, Copper material has the largest contribution to the environment, which is around 345,054 *euro*, while the impact from the Ferrite magnet is much lower, at 7,698 *euro*.

Table 4.10: Comparison of environmental impact of the Neodymium and the Ferrite machine [22]

Machine Model	Machine part	Material	Weight (kg)	ELU (euro/kg)	Total impact (euro)
Neodymium	Stator core	Steel	3,081	1	3,081
	Rotor core	Steel	18,240	1	18,240
	Winding	Copper	1,533	131	200,823
	Magnet	Neodymium	2,212	102.8	227,393
	Total		25,066	17.9	449,537
Ferrite	Stator core	Steel	5,778	1	5,778
	Rotor core	Steel	34,190	1	34,190
	Winding	Copper	2,634	131	345,054
	Magnet	Ferrite	2,654	2.9	7,698
	Total		45,256	8.7	392,718

4.10 Global warming potential analysis of the machines

Table 4.11 presents the Global Warming Potential (GWP) and material impact for the Neodymium and Ferrite machine. Both machines exhibit the same GWP per kilogram for the stator core, rotor core, and winding, which are 8.3 kgCO2-eq/kg for winding and 1.5 kgCO2-eq/kg for stator and rotor core[23]. However, the GWP for the neodymium magnet is five times higher than the ferrite magnet, 27.6 kgCO2-eq/kg for the neodymium magnet[24] and 5.1 kgCO2-eq/kg for the ferrite magnet[25]. Moreover, the significant differences arise in the total weight and corresponding material impact of the two models.

The Neodymium machine has a total weight of 25,066 kg, significantly lower than the Ferrite-based machine, which weighs 45,256 kg. This disparity is particularly pronounced in the rotor component, where the Ferrite rotor weighs 34,190 kg, nearly double that of the Neodymium rotor at 18,240 kg. Similarly, the stator in the Ferrite machine is considerably heavier than its Neodymium counterpart, weighing 5,778 kg compared to 3,081 kg. Although the Neodymium machine weighs 2 times lighter than the Ferrite machine, the total material impact produced by the Neodymium

machine is slightly higher. This is because the GWP of neodymium magnets is very high compared to ferrite magnets. The Neodymium model has a total material impact of 105,755 kgCO2-eq, slightly higher than the 95,349 kgCO2-eq impact of the Ferrite model. This comparison shows the environmental advantages of the Ferrite machine, which achieves lower overall material impact due to its lower GWP.

Table 4.11: Global Warming Potential of the material used for both machines for 30 years

Machine model	**Machine part**	**Material**	**GWP (kgCO2-eq/kg)**	**Weight (kg)**	**Material impact (kgCO2-eq)**
Neodymium	Winding	Copper	8.3	1,533	12,724
	Stator	Steel	1.5	3,081	4,622
	Rotor	Steel	1.5	18,240	27,360
	Magnet	Neodymium	27.6	2,212	61,051
	Total		**38.9**	**25,066**	**105,757**
Ferrite	Winding	Copper	8.3	2,634	21,862
	Stator	Steel	1.5	5,778	8,667
	Rotor	Steel	1.5	34,190	51,285
	Magnet	Ferrite	5.1	2654	13,535
	Total		**16.4**	**45,256**	**95,349**

Electricity generation in Sweden mostly is characterized by a remarkably low carbon intensity. For more details, the energy mix in Sweden consists of hydropower, 40% of total generation, nuclear power contributing around 29%. Additionally, wind, solar panels, bio-fuels and waste contribute to around 30%, while the rest comes from fossil fuels[26]. Moreover, Sweden has a low-carbon electricity profile at 19 gCO2-eq/kWh [27].

The low carbon intensity of Sweden's electricity grid significantly impacts the global warming potential (GWP) of the electric ships operation. By using the losses on the drive cycle, the electricity impact of the Neodymium and Ferrite machine can be calculated by,

$$\text{Electricity Impact}_{Neodymium} = 0.18 \text{ MWh x } 19 \text{ kgC02-eq/MWh} = 3.42 \text{ kgCO2-eq}$$

$$\text{Electricity Impact}_{Ferrite} = 0.24 \text{ MWh x } 19 \text{ kgC02-eq/MWh} = 4.56 \text{ kgCO2-eq}$$

Then, we can estimate the emission of the ship for 30 years,

$$\text{Electricity Impact}_{Neodymium} = 0.18 \text{ MWh x } 365 \text{ x } 30 \text{ x } 19 = 37,449 \text{ kgCO2-eq}$$

$$\text{Electricity Impact}_{Ferrite} = 0.24 \text{ MWh x } 365 \text{ x } 30 \text{ x } 19 = 49,932 \text{ kgCO2-eq}$$

Table 4.12: Total impact for both machines

Machine Model	**Material impact (kgCO2-eq)**	**Electricity impact (kgCO2-eq)**	**Total Impact (kgCO2-eq)**
Neodymium	105,757	37,449	143,206
Ferrite	95,349	49,932	145,281

Tabel 4.12 presents the total impact for both machines. It can be seen that the Ferrite machine slightly has higher of total impact for the environment, which is around 145,281 kgCO2-eq, while the Neodymium machine is 143,206 kgCO2-eq.

Finally, this emission value is significantly lower than that in Poland, where the emissions over the same period will be approximately 1,359,990 kgCO-eq for only the electricity impact for the Neodymium machine. This is because Poland's grid, with its higher reliance on coal for around 63%, results in greater emissions, at 690 gCO2-eq/kWh, compared to Sweden's low-carbon electricity system[28].

4.11 Ethical impact

Global warming is one of the most serious problems facing humanity today and we need to also consider it in the design of machines. In the previous chapters, we showed the material usage, the environmental load unit, and the calculation of the total environmental impact cost of the two materials of the machines. It can be seen that the mining and production of the Neodymium magnets have a great impact on the environment, and a large amount of carbon dioxide and other greenhouse gases will be released during the mining process, indirectly accelerating global warming. Therefore, we should not only use the Neodymium machine in applications that require extremely high efficiency and help reduce global warming, such as electric vehicles and wind power generation, but also research and develop new magnetic materials with less environmental impact that can replace the Neodymium and Ferrite.

5
Conclusions

This report investigates two machines for ship propulsion, the Neodymium, and the Ferrite, having a torque around of 200 kNm. Then, the design of the Neodymium machine is, as expected, more compact, 1440 mm of motor length, compared to the Ferrite machine, 2700 mm of motor length, to achieve similar results. This is because the magnet remanence of the Neodymium magnet is 1.125 Tesla, which is higher than that of the Ferrite magnet at 0.43 Tesla. This magnet remanence causes the high flux density possessed by the Neodymium machine compared to the Ferrite machine.

In the thermal analysis, the Neodymium machine shows higher winding temperatures, 106°C, compared to the Ferrite machine, 89°C. Although cooled by seawater, the Neodymium machine requires stronger cooling, especially for windings under higher thermal loads. In contrast, the Ferrite machine offers better thermal stability, making it more reliable in applications with limited cooling.

Regarding losses in both machines, the Neodymium machine contributes to a total loss of 64.19 kW, which is lower than the Ferrite machine at 95.34 kW. The stator copper loss of the Neodymium machine is 40.66 kW, while the Ferrite machine has a significantly higher copper loss at 69.85 kW. This difference is caused by the resistance in the Ferrite being higher than the Neodymium model, contributing to the high copper losses, in which the resistance of the Neodymium and Ferrite machine are 0.020 Ohms and 0.042 Ohms, respectively.

The efficiency data show that the maximum efficiency of the Neodymium machine is 95.9%, while the maximum efficiency of the Ferrite machine is 94.1%. Moreover, the the drive cycle operation shows that the Ferrite machine has higher losses, 0.24 MWh, and slightly higher energy consumption, 4.68 MWh, than the Neodymium machine, which are 0.18 MWh and 4.59 MWh, respectively. From the perspective of the electromagnetic performance of the machine, the advantages of the Neodymium machine are far greater than those of the Ferrite machine.

The environmental impact was evaluated using the EPS and GWP. The Neodymium machine has a higher environmental impact at 449,537 euro compared to the Ferrite machine at 392,718 euro, resulting higher compensation for the environmental damage for the Neodymium machine than the Ferrite machine. In the GWP analysis, although the Neodymium machine has less total material weight, it results higher total material impact than the ferrite machine due to the higher GWP of the

neodymium magnet at 27.6 kgCO2-eq compared to 5.1 kgCO2-eq for the ferrite magnet. Then, the total impact for the Neodymium magnet is 143,206 kgCO2-eq compared to 145,281 kgCO2-eq of the Ferrite machine. This is because the Neodymium machine produces lower losses during the ship operational. Finally, Sweden has a low-carbon electricity of 19 gCO2-eq/kWh, resulting in lower emissions compared to the emission in Poland of 690 gCO-eq/kWh.

5.1 Future Work

Further improvement for the machines will improve the overall performance from wider aspects such as materials, structure, thermal management, intelligent control, and application expansion, ensuring its competitiveness and sustainability in future high-demand scenarios.

Firstly, improvement and optimization in materials are important for future application. Although two magnetic materials have been used, the application of new rare-earth alloys, nanomaterials, and environmentally friendly composite materials to replace the rare earth metals, which can help reduce the carbon footprint and manufacturing costs.

Secondly, research on thermal management and cooling technology will significantly affect the performance and lifespan of the machine. In the future, the study can be managing the heat conduction path inside the machine, further optimize the heat dissipation structure, or develop new cooling methods such as liquid cooling to improve the efficiency of the temperature system to ensure the stable operation under long-term and high-load conditions.

Finally, the optimization of intelligent control strategies will be an important trend in future development. With the development of artificial intelligence and machine learning, research on intelligent control algorithms, such as AI-based dynamic control, can automatically adjust current and voltage according to real-time working conditions, further improving efficiency and reducing energy consumption, thereby achieving intelligent energy management.

Bibliography

[1] R. Lateb, N. Takorabet, F. Meibody-Tabar, A. Mirzaian, J. Enonand A. Sarribouette, “Performances comparison of induction motors and surface mounted PM motor for POD marine propulsion”, vol. 2, pp. 1342–1349. doi: 10.1109/ias.2005.1518534.

[2] Y. Zhang, S. Mcloone, W. Cao, F. Qiuand C. Gerada, “Power Loss and Thermal Analysis of a MW High-Speed Permanent Magnet Synchronous Machine”, IEEE Transactions on Energy Conversion, vol. 32, no. 4, pp. 1468–1478, 2017, doi: 10.1109/tec.2017.2710159.

[3] Y. Tang, S. Sun, W. Yuand W. Hua, “Thermal Analysis of Water-Cooling Permanent Magnet Synchronous Machine for Port Traction Electric Vehicle”, Electronics, vol. 12, no. 3, p. 734, 2023, doi: 10.3390/electronics12030734.

[4] O. Dobzhanskyi, V. Grebenikov, R. Gouws, R. Gamaliiaand E. Hossain, “Comparative Thermal and Demagnetization Analysis of the PM Machines with Neodymium and Ferrite Magnets”, Energies, vol. 15, no. 12, p. 4484, 2022, doi: 10.3390/en15124484.

[5] F. Montenero and V. Petkov, "Design and thermal management of high-performance Neodymium-based PMSMs for naval propulsion," Journal of Marine Science and Technology, vol. 21, no. 3, pp. 465-474, 2016. doi: 10.1007/s00773-015-0340-4.

[6] International Towing Tank Conference, "Recommended Procedures and Guidelines: Podded Propulsor Test Procedure," 26th ITTC, 2011. [Online]. Available: https://ittc.info/media/1217/75-02-02-01.pdf. [Accessed: Oct. 25, 2024].

[7] Yujing Liu et al. "Electrical Machines - Design and Analysis 1st Edition", Chalmers University of Technology, 2019.

[8] "Rounded Rectangle Area and Perimeter Calculator," HAD2KNOW. [Online]. Available: https://www.had2know.org/academics/rounded-rectangle-area-perimeter.html. [Accessed: Nov. 14, 2024].

[9] J. Lindström, “Development of an experimental permanent-magnet motor drive,” Licentiate of Engineering, Technical Report No. 312L, Chalmers University of Technology, apr 1999.

[10] Juha Pyrhonen et al. "Design of Rotating Electrical Machines 2", Chicester: Wiley, 2010.

[11] W. Dongxin, “Design and Temperature Field Analysis of Submersible Motor”, 2020. doi: 10.1109/icectt50890.2020.00037.

[12] Schüler, D., et al. (2011). "Critical metals for future sustainable technologies and their recycling potential." United Nations Environment Programme (UNEP).

[13] P. Gómez, D. Elduque, C. Pinaand C. Javierre, “Influence of the Composition on the Environmental Impact of Soft Ferrites”, Materials, vol. 11, no. 10, p. 1789, 2018, doi: 10.3390/ma11101789.

[14] Berg, L., & Helldén, U. (2007). Electrical systems in pod propulsion (Master’s thesis). Chalmers University of Technology. Available at: https://hdl.handle.net/20.500.12380/64477.

[15] How Does Temperature Affect Neodymium Magnets.FIRST4MAGNETS .https://www.first4magnets.com/tech-centre-i61/information-and-articles-i70/neodymium-magnet-information-i82/how-does-temperature-affect-neodymium-magnets-i91.pdf

[16] Bhatia A. Understanding Motor Nameplate Information: NEMA vs. IEC Standards[J]. Continuing Education and Development Inc, 2022.

[17] A. O. Di Tommaso, F. Genduso, R. Miceli and C. Nevoloso, "Fast procedure for the calculation of maximum slot filling factors in electrical machines," 2017 Twelfth International Conference on Ecological Vehicles and Renewable Energies (EVER), Monte Carlo, Monaco, 2017, pp. 1-8, doi: 10.1109/EVER.2017.7935906.

[18] M. Butković, B. Orčić, and M. Tevčić, "Consideration of safety factors for cyclic stressed machine parts calculated with FE method - Case study," in International Design Conference - DESIGN 2004, Dubrovnik: Fakultet strojarstva i brodogradnje Sveučilišta u Zagrebu, 2004, pp. 1205–1212.

[19] G. Chu, R. Dutta, M. F. Rahman, H. Lovatt and B. Sarlioglu, "Analytical Calculation of Maximum Mechanical Stress on the Rotor of Interior Permanent-Magnet Synchronous Machines," in IEEE Transactions on Industry Applications, vol. 56, no. 2, pp. 1321-1331, March-April 2020, doi: 10.1109/TIA.2019.2960756.

[20] E. A. Grunditz, S. T. Lundmark, M. Alatalo, T. Thiringerand A. Nordelof, “Three traction motors with different magnet materials — Influence on cost, losses, vehicle performance, energy use and environmental impact”, 2018, vol. 63, pp. 1–13. doi: 10.1109/ever.2018.8362387.

[21] J. Dai, Y. Dai, Z. Wangand H. Gao, “Preparation and magnetic properties of lanthanum- and cobalt-codoped M-type strontium ferrite nanofibres”, Journal of Experimental Nanoscience, vol. 10, no. 4, pp. 249–257, 2015, doi: 10.1080/17458080.2013.824618.

[22] G. Cutuli, D. Barater, S. Nateghand B. Raghuraman, “Aluminum Hairpin Solution for Electrical Machines in E-Mobility Applications : Part I: Electromagnetic Aspects”, 2022. doi: 10.1109/icem51905.2022.9910945.

[23] P. Nuss and M. J. Eckelman, “Life Cycle Assessment of Metals: A Scientific Synthesis”, PLOS ONE, vol. 9, no. 7, p. e101298, 2014, doi: 10.1371/journal.pone.0101298.

[24] H. Jin, P. Afiuny, T. McIntyre, Y. Yih, and J. W. Sutherland, “Comparative Life Cycle Assessment of NdFeB Magnets: Virgin Production versus Magnet-to-Magnet Recycling,” Procedia CIRP, vol. 48, pp. 45–50, 2016, doi: 10.1016/j.procir.2016.03.013.

[25] A. Amato et al., “Life Cycle Assessment of Rare Earth Elements-Free Permanent Magnet Alternatives: Sintered Ferrite and Mn–Al–C,” ACS Sustainable

Chem. Eng., vol. 11, no. 36, pp. 13374–13386, Sep. 2023, doi: 10.1021/acssuschemeng.3c02984.

[26] International Energy Agency, "Sweden Electricity," IEA. [Online]. Available: https://www.iea.org/countries/sweden/electricity. [Accessed: Nov. 29, 2024].

[27] Nowtricity, "Sweden Electricity Profile," Nowtricity. [Online]. Available: https://www.nowtricity.com/country/sweden. [Accessed: Nov. 29, 2024].

[28] Nowtricity, "Polan Electricity Profile," Nowtricity. [Online]. Available: https://www.nowtricity.com/country/poland/ [Accessed: Nov. 29, 2024].

[29] Callister, W. D. (2007). Materials Science and Engineering: An Introduction (8th ed.). John Wiley Sons

A

Material specification

A.1 M800-50A

Table A.1 shows the properties of M800-50A and Table A.2 shows the B-H curve of material M800-50A, which is obtained from the Motorcad database.

Table A.1: M800-50A properties

Property	**Value**	**Unit**
Density	7650	kg/m^3
Electrical Resistivity	2.3×10^{-7}	Ohm ·m
Thermal Conductivity	30	W /m / °C
Eddy current loss coefficient,Kc	0.65	
Hysteresis loss coefficient,Kh	0.05318	

Table A.2: B-H Curve for M800-50A

H (Amps/m)	**B** (Tesla)
0.0	0.0
0.1	49.4217
0.3	118.7541
0.5	146.0186
0.7	168.252
0.9	195.0656
1.1	237.706
1.3	345.8256
1.5	1046.9084
1.7	4944.6712
1.8	9210,2309

A.2 Copper

Table A.3 shows the properties of Copper, which is obtained from the [30] and Motorcad database.

Table A.3: Copper properties

Property	Value	Unit
Density	8933	kg/m^3
Electrical Resistivity	1.724×10^{-8}	Ohm·m
Electrical Conductivity	5.8×10^7	Siemens/m
Thermal Conductivity	401	W /m / °C

A.3 Milled steel

Table A.4 shows the properties of Milled Steel, which is obtained from the Motorcad database.

Table A.4: Milled properties

Property	Value	Unit
Density	7800	kg/m^3
Electrical Resistivity	1.42×10^{-7}	Ohm ·m
Thermal Conductivity	25	W /m / °C
Kh	0.65	

A.4 Neodymium (N30UH)

Table A.5 shows the properties of Neodymium, which is obtained from the Motorcad database.

Table A.5: Neodymium (N30UH) properties

Property	Value	Unit
Density	7500	kg/m^3
Electrical Resistivity	1.8×10^{-7}	Ohm ·m
Thermal Conductivity	7.6	W /m / °C
Remanent flux density,B_r	1.125	
Tesla Coercive force,H_c	1990	kA/m
Poisson's ratio	0.24	
Young's Modulus	160	GPa

A.5 Ferrite (Y34)

Table A.6 shows the properties of Ferrite, which is obtained from the Motorcad database.

Table A.6: Ferrite (Y34) properties

Property	Value	Unit
Density	4800	kg/m^3
Electrical Resistivity	100	Ohm ·m
Thermal Conductivity	13.4	W /m / °C
Remanent flux density,B_r	0.43	
Tesla Coercive force,H_c	220	kA/m
Poisson's ratio	0.28	
Young's Modulus	160	GPa

DEPARTMENT OF Electrical Engineering
CHALMERS UNIVERSITY OF TECHNOLOGY
Gothenburg, Sweden
www.chalmers.se

CHALMERS
UNIVERSITY OF TECHNOLOGY